JOURNAL OF AIRCRAFT
Vol. 44, No. 5, September–October 2007

Early Flight-Test and Other Boundary-Layer Research at Mississippi State 1949–1960

David H. Bridges*
Mississippi State University, Mississippi State, Mississippi 39762

DOI: 10.2514/1.28086

In 1949, August Raspet was hired by Mississippi State College to establish a research program in aerophysics. Raspet and coworkers began a series of experiments in boundary layers and other viscous flows that led to a number of discoveries, in particular the effectiveness of distributed suction in delaying transition and preventing separation. A number of these studies were conducted using gliders and modified general aviation aircraft. Eventually, two prototype aircraft were constructed that combined all of the technologies previously studied. This study surveys the boundary-layer research that led up to these prototype aircraft and discusses some of the technologies developed. The experimental techniques used are also discussed.

I. Introduction

IN 1948, the Dean of the School of Engineering at Mississippi State College, L. L. Patterson, hired Harold von Neufville Flinsch as a professor of civil engineering and associate director of the Engineering and Industrial Research Station (EIRS), with the understanding that Flinsch would become dean and director of EIRS upon Patterson's retirement. When he became dean in 1949, Flinsch was given two primary duties: increase the number of faculty with terminal degrees and expand the research programs in the School of Engineering. Budgetary and other constraints prevented rapid progress on the first goal. However, Flinsch could do something almost immediately about the second. Flinsch, a pilot and a sailplane enthusiast, was familiar with sailplane research in Germany before World War II (WWII) that had led to advances in aircraft technology, and had made particular note of the fact that such research could be done relatively inexpensively. He reasoned that if certain universities in Germany with limited means could conduct such research, there was no reason why Mississippi State College could not have a similar program. The effort to begin such a program brought him into contact with Dr. August Raspet (1913–1960).

Raspet (Fig. 1) had graduated from the Carnegie Institute of Technology and had gone on to receive a Ph.D. in physics from the University of Maryland in 1942. Like Flinsch, Raspet was a sailplane enthusiast and had achieved some recognition in this area. In 1946, he served as director of the research phase of the Thunderstorm Project, in which he and other pilots flew sailplanes into thunderstorms. The motions of the sailplanes were tracked on radar, yielding information about the wind currents within the storms. After the Thunderstorm Project, he moved to New York, where he became the director of the Aerophysics Institute and began work on a grant from the Office of Naval Research. The purpose of this study was to use sailplanes to study airflow patterns over mountain ridges. Flinsch contacted Raspet about moving to Mississippi State and beginning his own independent sailplane research program, which he did in February of 1949. The Aerophysics Department was created by Flinsch just for Raspet and his sailplane research [1,2].

Presented as Paper 1121 at the 44th AIAA Aerospace Sciences Meeting and Exhibit, Reno, NV, 9–12 January 2006; received 29 September 2006; revision received 20 December 2006; accepted for publication 27 December 2006. Copyright © 2007 by David H. Bridges. Published by the American Institute of Aeronautics and Astronautics, Inc., with permission. Copies of this paper may be made for personal or internal use, on condition that the copier pay the $10.00 per-copy fee to the Copyright Clearance Center, Inc., 222 Rosewood Drive, Danvers, MA 01923; include the code 0021-8669/07 $10.00 in correspondence with the CCC.

*Associate Professor, Department of Aerospace Engineering, P. O. Drawer A. Senior Member AIAA.

II. Experimental Methods

The primary platform used for the early boundary-layer research at Mississippi State was the Schweizer TG-3A sailplane (see Fig. 2). The school had four of these World War II surplus gliders that had been used to train Army glider pilots during the war. The TG-3A had a wingspan of 52 ft, a length of 27.6 ft, a wing area of 233.3 ft^2, an aspect ratio of 11.5, and a maximum weight of 700 lb [3,4]. The aircraft had an NACA 4416 airfoil section. Figure 3 shows a cross section of the wing of the TG-3A [5]. The front "D-ring" was formed by a plywood sheet and the main spar whose trailing edge was at $x/c = 0.345$. Aft of the main spar, the wing was covered with fabric. In the early experiments, the plywood was left impervious and only the fabric was perforated. Later, the plywood was also drilled with holes.

The earliest experiments on boundary layers were in the area of boundary-layer transition. The principal instrument used to detect transition was a stethoscope attached to a flattened Pitot probe. The photograph of Raspet in Fig. 1 shows him wearing a stethoscope. The technique is illustrated in Fig. 4 and discussed in [6]. The probe was moved along the surface of the wing, which was marked for distance, and the investigator listened for a change in the sound. According to Raspet, "[t]he sound heard in the stethoscope in the laminar region is a gentle hiss, but in the turbulent boundary layer a loud roar, similar to a frying noise, is heard. The contrast is so sharp that there is little subjective error in defining the zone of transition. In regions of low boundary-layer stability infrequent bursts of turbulence may be heard. As one approaches the transition zone these bursts get more and more frequent until they merge into complete turbulence [7]." Later, a "balanced microphone," an electronic version of the stethoscope, was developed for more detailed stability and transition studies [8]. It saw limited use in basic transition detection, being used to determine the location of an increase in sound level, but was not developed further.

Other devices used in boundary-layer studies were the boundary-layer "mouse" shown in Fig. 5 and an "integrating mouse" (not shown). The mouse was a standard device for measuring boundary-layer velocity profiles. The mouse was attached to the wing at a specific chordwise location and the aircraft was flown through a set of conditions. The pressures measured by the probes in the mouse were recorded by photographing a "U"-tube manometer bank in the cockpit of the glider. The mouse was then moved to a different chordwise position and the aircraft was flown through the same set of conditions. In this manner the boundary-layer profiles on the wing were obtained [9]. The integrating mouse was also used to obtain the momentum thickness [10]. The difference Δp between the integrated pressure from the rake and the freestream stagnation pressure was measured. The analysis presented by Cornish [10] showed that if a value of the shape parameter H of 1.4 was assumed for a turbulent boundary layer, then the momentum thickness θ was

Fig. 1 August Raspet.

Fig. 2 Schweitzer TG-3A sailplane used for boundary-layer research at Mississippi State.

approximately equal to $\Delta ph/(1.2\rho U^2)$, where h was the total height of the device. Cornish pointed out that the measures so obtained were only used in a relative sense, primarily to determine the optimum pressure difference across the perforated skin.

Figure 6 shows a device called the "shear meter." The shear meter worked in a manner similar to a Preston tube [5]. By measuring the pressure difference at a known height above the surface, a corresponding velocity could be calculated. The shear stress at the wall was known to be proportional to this velocity through a Preston-type correlation (Fig. 12 in [5]). Often the velocity was used as an indicator of the shear stress, because often only relative values of shear stress were desired, usually to indicate separation. The shear meter was free to rotate about its vertical axis, and the vane at the rear kept the shear meter pointed into the relative wind. The shear meter was traversed manually across the wing surface in the same manner as the stethoscopes (both manual and electric versions). A similar

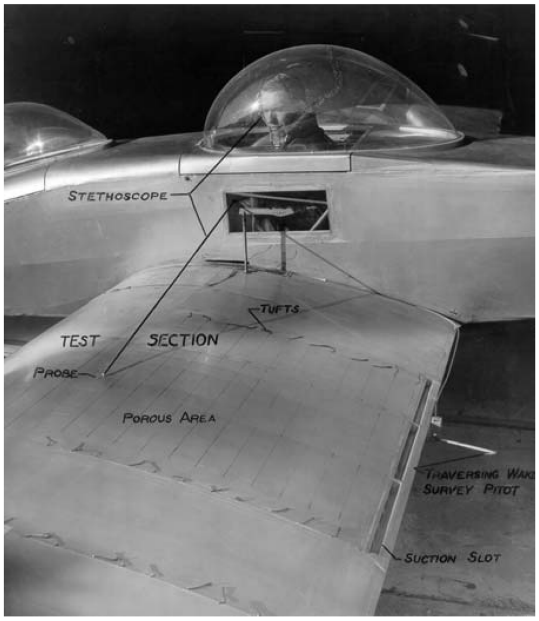

Fig. 4 Illustration of use of stethoscope in detecting boundary-layer transition (from [6]).

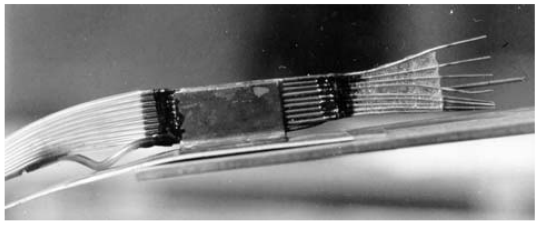

Fig. 5 Boundary-layer mouse (from [5]).

"flying probe" was used to obtain the velocity distribution just outside the boundary layer by measuring the difference between the static and stagnation pressures [10].

Figure 4 also shows a traversing Pitot probe. This device was used to obtain the wake stagnation pressure profile behind the wing. This profile was integrated to obtain the profile drag of the wing section [6]. Tufts and sublimation of dew or naphthalene were used to observe transition and/or separation. Tufts may been seen in Fig. 4; an example of dew sublimation will be shown later.

III. Boundary-Layer Transition Studies

A. Initial Empirical Studies

The first research report issued by Raspet [6,11] described an attempt to augment the lift coefficient and reduce the drag of a sailplane by the use of a suction slot at the trailing edge of the wing. This followed work by Betz [12] who had shown using potential flow theory that for a rounded trailing-edge airfoil, the lift coefficient could be set by setting the location of the rear stagnation point. According to the report by Raspet [6], Regenscheit [13] had done some work showing that, in addition to augmenting the lift coefficient, the trailing-edge suction could also be used to decrease

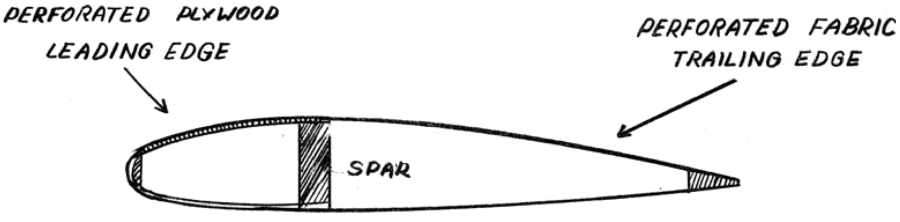

Fig. 3 Cross section of TG-3A wing (Fig. 5 in [10]).

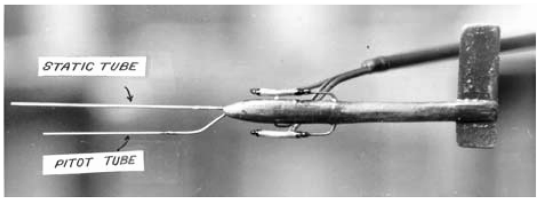

Fig. 6 Photograph of shear layer meter (from [5]).

the profile drag of the airfoil by reducing or eliminating separation at the trailing edge. Regenscheit had used for his suction source the low pressure region near the tip of the wing, hence his term "automatic suction." Smith [14] had also performed some similar calculations on the effects of trailing-edge suction on lift and drag. The purposes of Raspet's study were to explore the effects of trailing-edge suction on boundary-layer transition for the purposes of drag reduction, to examine the issue of lift augmentation, to optimize the automatic suction effect by determining the appropriate location on the wing tip for the suction source, and to investigate the effects of distributed suction on boundary-layer stabilization.

The tests were conducted using the TG-3A sailplane previously described. The location of boundary-layer transition was determined using the stethoscope method. The suction was provided using a battery-powered motor located in the cockpit. The trailing-edge suction studies showed that trailing-edge suction had little if any effect on boundary-layer transition, and Raspet concluded that the effects of trailing-edge suction did not extend far enough forward to influence the laminar boundary layer, and, therefore, any drag reduction from trailing-edge suction must come from reducing the profile drag by reducing boundary-layer separation. The lift augmentation studies showed an amplification factor $\Delta C_L/C_Q$ of 6.7, where $C_Q = Q/VS$ was the suction coefficient and ΔC_L was the increment in lift due to the application of suction. This low value compared with some other values was attributed to the suction slot not extending the full span of the wing and the slot design not being an optimum design. The automatic suction research was a bit more fruitful. Pressure measurements on the upper surface of the glider wing at a lift coefficient of 1.16 yielded a region where the suction pressure was $1.6q$, where q was the dynamic pressure.

By far the most fruitful phase of this research was the study of the effects of distributed suction on boundary-layer stability and transition. Raspet [6] noted that the computations by Smith [14] that had predicted improvements in lift coefficient with trailing edge suction had been potential flow calculations, and so he reasoned that a laminar boundary layer might more closely match the flow computed by Smith. The use of distributed suction to achieve laminar flow had been suggested by theoretical works by Ulrich [15], Schlichting [16], and Iglish [17], all indicating that the application of a suction velocity on the order of 10^{-4} times the freestream velocity would stabilize the boundary layer on a flat plate. Raspet cited works by Pfenninger [18,19] and by Burrows et al. [20,21] as examples of boundary-layer stabilization by suction through slots and porous media, respectively. The work performed by Raspet's group was then discussed. The distributed suction experiments were performed on the wing of the TG-3A glider discussed previously (see Fig. 3). For these tests described in [6], the plywood portion was left impervious and holes were punched only in the fabric portion of the wing cover. The plywood portion was smoothed to a waviness of less than ± 0.002 in to remove possible trips so that the boundary layer would remain laminar to a point past the spar where suction could be applied. When the leading-edge spar cap was made smooth, the boundary layer was laminar to a point just past the trailing edge of the spar at $x/c = 0.345$ for all aircraft lift coefficients below 0.93. This meant that any suction applied to the portion of the wing behind the spar that maintained laminar flow over the rest of the wing should be able to do it for all lift coefficients below 0.93. For this phase of the tests, where only the fabric portion of the wing aft of the spar was to be perforated, maintaining a laminar boundary layer to that point was critical, because as Raspet quoted Pfenninger [18] as stating, no amount of suction would relaminarize a turbulent boundary layer.

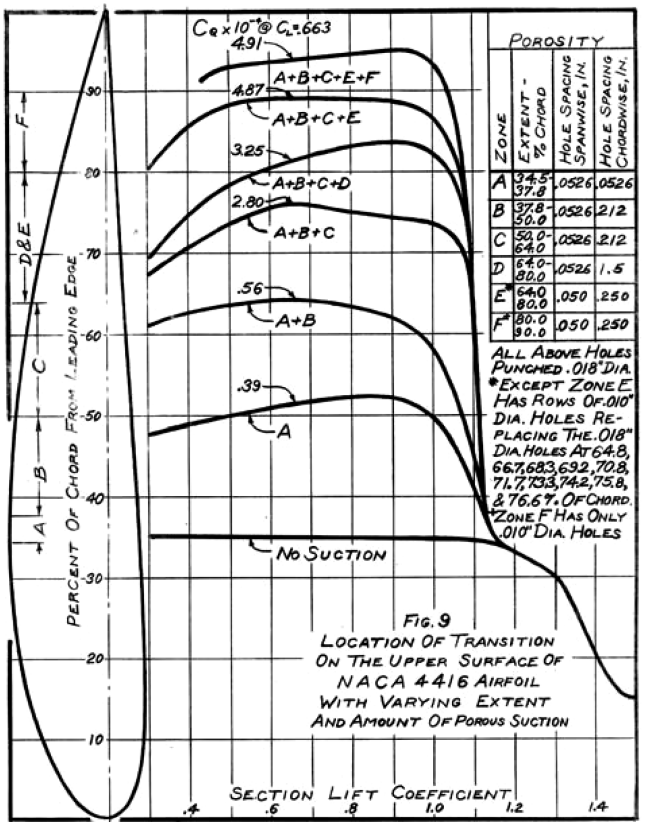

Fig. 7 Effects of suction on boundary-layer transition location (Fig. 9 in [6]).

Hence, to maintain a laminar boundary layer with distributed suction, the initial boundary layer would have to be laminar.

Figure 7 (Fig. 9 in [6]) shows the effects of the application of different zones of suction. This figure shows the transition location as a function of airplane lift coefficient for each of the different suction zones applied. This figure was achieved through a "punch and try" method. A zone of holes was added to the wing. Suction was applied to the holes and the extent of the laminar boundary layer was determined. This information was used to determine where the next zone of holes should be applied (how far back and what spacing). The numerical label on each curve is the cumulative suction coefficient C_Q which includes the total suction on the wing for the combination of zones represented by each curve. The curve labeled "no suction" is of interest. It is for the set of holes labeled "zone A" but with the suction motor turned off. It is apparent from this curve that transition occurs immediately behind the trailing edge of the spar, where the

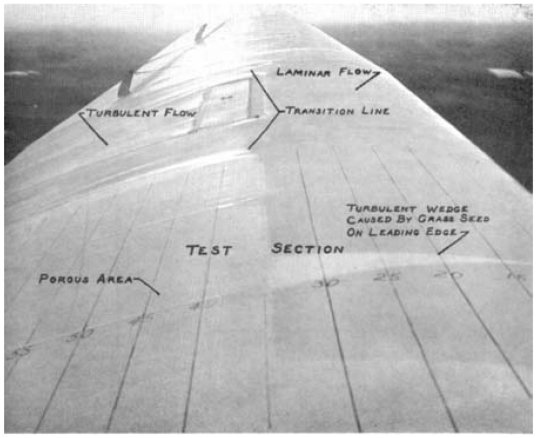

Fig. 8 Transition on wing with suction off illustrated by dew evaporation (Fig. 9a in [6]).

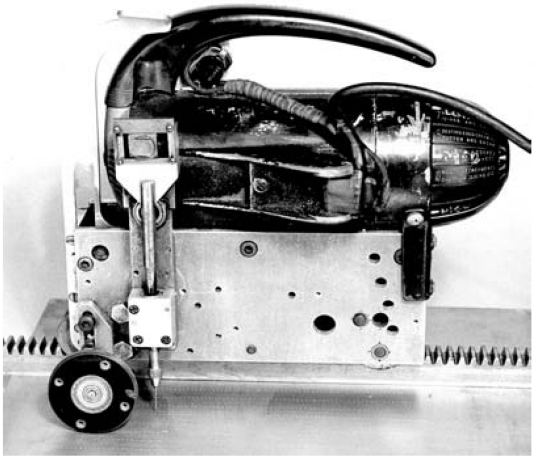

Fig. 9 Fabric hole punch device.

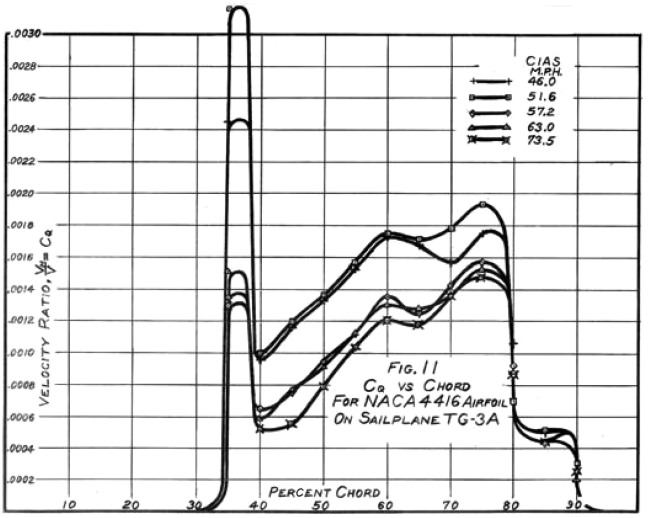

Fig. 10 Suction distribution on wing for first suction stabilization study (Fig. 11 in [6]).

suction holes began. In the report, this curve was compared with a curve for the impervious wing generated during the trailing-edge suction tests. At the lower lift coefficients, the boundary layer on the impervious wing was laminar up to a distance of $x/c = 0.45$ from the leading edge. With the suction motor off, there was outflow from the holes in the fabric and this outflow destabilized the boundary layer, causing it to transition as soon as the perforated region was reached. This is demonstrated by the flow visualization picture shown in Fig. 8 (Fig. 9a in [6]). This photograph shows the evaporation of dew from the wing and illustrates dramatically the transition line at $x/c = 0.345$.

The holes in zone A were distributed with a spanwise separation of 0.0526 in. and a chordwise separation of 0.0526 in. The hole diameter was 0.018 in. and the holes were punched using the device shown in Fig. 9. This device could punch 15 holes per second in doped fabric. The hole diameter was determined by the size of the needle inserted into the device. Zone A extended only for $0.345 < x/c < 0.378$, but the application of suction through this zone produced laminar flow as far back as $x/c = 0.53$. This rather dense spacing of holes immediately behind the trailing edge of the spar was thought to be necessary to restore the "health" of the laminar boundary layer after it had traversed the leading edge and spar cap and was beginning to enter the adverse pressure gradient on the rear of the airfoil. The next set of holes (zone B) used the same spanwise spacing but increased the chordwise spacing to 0.212 in., a factor of four greater than in zone A. This zone extended through $0.378 < x/c < 0.5$ and zones A and B together produced laminar flow as far back as $x/c = 0.64$. Zone C maintained the same spanwise and chordwise spacing, extended through $0.5 < x/c < 0.64$, and zones A–C together produced laminar flow as far back as $x/c = 0.75$. This led to a chordwise spacing in zone D of 1.5 in. which extended through $0.64 < x/c < 0.80$. Zones A–D together produced laminar flow only as far back as $x/c = 0.85$. It was recognized that if the same 1.5-in. spacing were maintained, the boundary layer would not be laminar when it reached the first row of the new zone. The chordwise spacing in zone D was reduced to 0.5 in., and the hole diameter was reduced to 0.01 in., creating zone E, but the extent of laminar flow was not increased significantly. Zone E was modified again to reduce the chordwise spacing to 0.25 in., and a new zone F was created extending through $0.8 < x/c < 0.9$. With suction applied to zones A–F inclusive, laminar flow was maintained on the wing to $x/c = 0.95$ with a suction coefficient $C_Q = 4.91 \times 10^{-4}$ at a lift coefficient $C_L = 0.663$. This value of C_Q was approximately a factor of four greater than the value computed by Ulrich [15] for a flat plate.

The resulting suction distribution is shown in Fig. 10 (Fig. 11 in [6]). This figure illustrates the large amount of suction applied just behind the spar and then the gradually increasing suction for $0.4 < x/c < 0.8$. The gradually increasing suction can be explained by the fact that the wing had a single internal cavity and, therefore, a single internal suction pressure. This pressure had to be set low enough so that at the point on the wing of maximum external suction, caused by the velocity distribution on the outside of the wing, the internal suction was greater than the external suction, so that there was an inflow into the wing. As the pressure increased on the outside of the airfoil past the suction peak, the pressure differential between the inside and outside was greater, causing more air to be drawn into the wing, thus causing the resulting local flow rate Q to rise. The amount of suction applied to the inside of the wing was varied with the airspeed, with higher amounts of suction being applied at higher speeds and the corresponding higher values of the external suction. The dropoff in suction rate toward the trailing edge of the wing was caused by the smaller hole diameter used in the final zone of the wing.

Figure 11 (Fig. 12 in [6]) shows the extent of the laminar flow region as a function of the wing internal pressure. The critical idea in this figure is the limited range of wing internal pressures for which

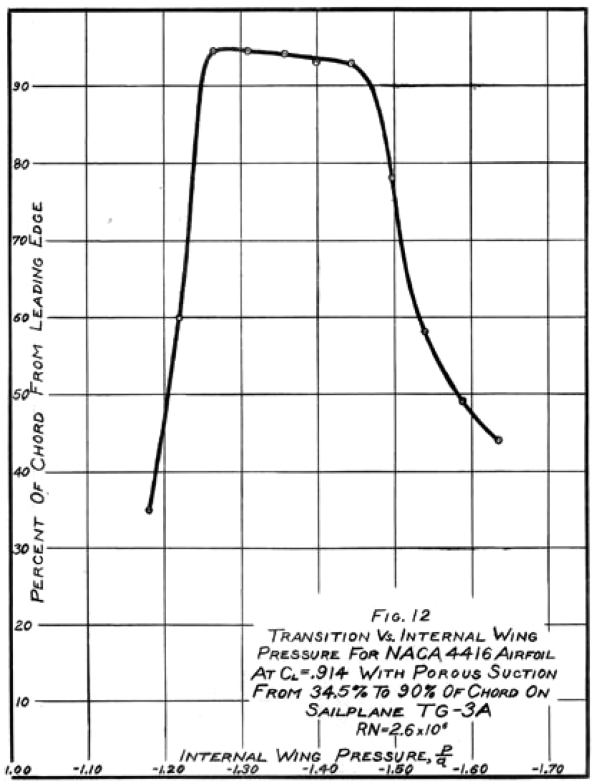

Fig. 11 Transition location as a function of wing internal pressure (Fig. 12 in [6]).

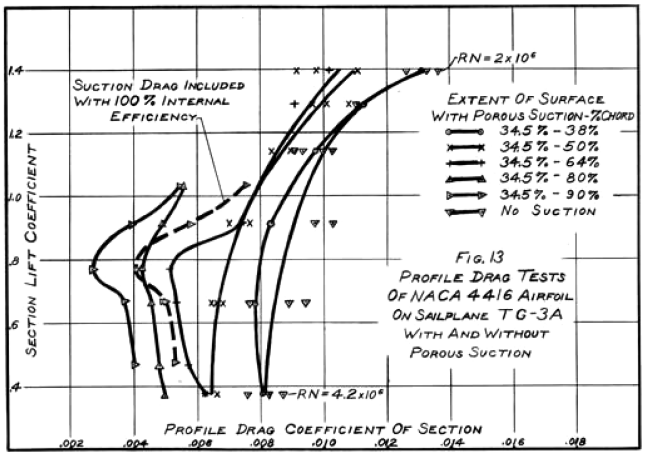

Fig. 12 Section drag polars for TG-3A showing effect of distributed suction on airfoil profile drag (Fig. 13 in [6]).

fully-laminar flow (up to $x/c = 0.93$ or greater) was obtained. These data were obtained at a lift coefficient of 0.914. The extent of the laminar flow region increased rapidly once the internal pressure reached $-1.28q$, where q is the freestream dynamic pressure. However, this maximum extent of laminar flow was only maintained to an internal pressure of approximately $-1.44q$. It is easy enough to understand the stabilizing effect of the suction as the internal pressure was made more negative (or, conversely, the destabilizing effect of outflow from the wing when the internal suction pressure was not low enough). However, the reasons for the decrease in the extent of the laminar flow region for internal pressures of magnitudes greater than $1.44q$ were not so clear. It was conjectured [6] that at large negative values of the wing internal pressure, the suction through the holes on the wing was creating crossflow patterns that were destabilizing the boundary layer. It was also conjectured that the higher suction values were distorting the fabric-covered portion of the wing, creating surface disturbances that were tripping the boundary layer. It was hoped that future tests would reveal the reasons for the destabilization of the boundary layer at the larger values of internal suction.

The effects of distributed suction on the airfoil section drag polars are shown in Fig. 12 (Fig. 13 in [6]). The drag coefficients were obtained using the traversing pitot probe discussed earlier and shown in Fig. 4. The polar on the left is for the maximum extent of laminar boundary-layer flow. The dashed line is the same polar with an effective drag coefficient of the suction system included. The blower and duct efficiencies were assumed to be 100%, but the actual

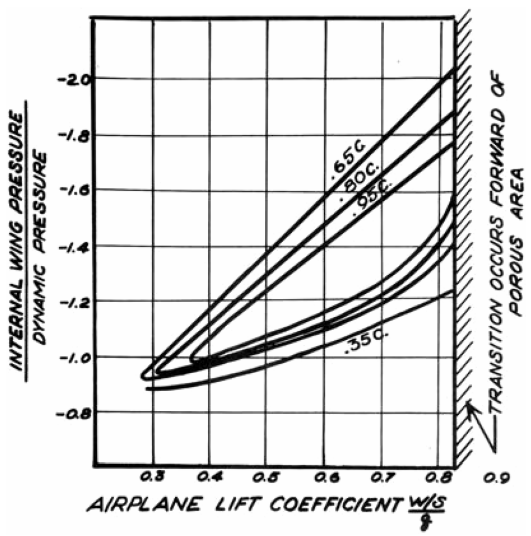

Fig. 13 Internal pressure/lift coefficient map for varying extents of boundary-layer stabilization (Fig. 1 in [9]).

pressure drop of the flow entering the wing was used to compute the power required for suction and then converted into an effective drag coefficient. This figure shows an approximately 50% decrease in the profile drag of the wing as a result of the application of distributed suction on the upper surface of the wing, even with the power required to produce the suction taken into account.

The next phase of the transition research [9,22] was led by Bruce Carmichael, an engineer working under Raspet, and began with an effort to determine the complete minimum and maximum suction pressure limits for maximum laminar flow extent for the original porosity distribution. The results of these tests are shown in Fig. 13 (Fig. 1 in [9]). The abscissa in this plot is the airplane lift coefficient (determined from a knowledge of the glider's weight, altitude, and airspeed), and the ordinate is the wing internal pressure as a fraction of freestream dynamic pressure (recall that the transition curve shown in Fig. 12 was for a single value of the lift coefficient). The region encompassed by the $0.95c$ contour represents those combinations of lift coefficient and internal pressure for which "full" stabilization was achieved. The boundary on the right is the lift coefficient at which the transition location moved forward of the trailing edge of the spar (and for some reason was at a lift coefficient of approximately 0.83, lower than the value of 0.93 reported in [6] and discussed before; the reason for the difference was not reported). The upper portion of the contour represents the boundary where increased suction pressure tended to destabilize the boundary layer, as discussed previously. At low lift coefficients, corresponding to high flight speeds, the upper and lower boundaries converge, implying that there was *no* value of the internal suction pressure that would produce full stabilization of the boundary layer. The issues of no full stabilization at high suction pressures and at low lift coefficients prompted the study which made up the remainder of the report by Carmichael [9,22].

Carmichael first discussed the determination of the pressure differential across the skin of the wing section [9,22]. The flying static probe was used to survey the difference between internal and external pressures for different settings of the wing internal pressure, and it was discovered that for settings which prevented outflow in the forward porous region where the external suction pressure was lowest, the pressure difference at the trailing edge was very large, and the problem became more severe as the airspeed increased. Carmichael concluded that the two problems of destabilization, at high internal suction pressure and at high speeds, were really the same problem.

The pressure differential method just discussed was used to determine the inflow velocity distribution [9,22]. The measured pressure differences were applied to the corresponding row of holes with the glider on the ground and the flow rate through the holes was measured with a variable area flow meter. Although there was some variation among hole rows, representative average values were obtained and these were reported. New porosity distributions were created. These began with the same basic principle as before, where a large inflow was applied just after the spar, to rejuvenate the boundary layer after its traverse of the impervious region ahead of the spar. Again, the extent of laminar flow for each portion of the distribution was used to determine the porosity of the next zone. This porosity distribution is shown in the dashed curve at the bottom of Figs. 14 and 15 (Figs. 4 and 5 from [9]). A second porosity distribution with reduced inflow was created by decreasing the hole diameter. This porosity distribution is shown in the solid curve at the bottom of Figs. 14 and 15.

It was recognized that to understand the limitations of the distributed suction method, more information about the actual behavior of the boundary layer than whether it was laminar or turbulent was needed. The boundary-layer properties were measured using the boundary-layer mouse (Fig. 6). The results of these measurements are shown in Figs. 14 and 15. In each of these figures, each of the two internal suction pressures shown was the minimum amount required to obtain "complete" stabilization (i.e., stabilization to $x/c = 0.95$) for each of the two porosity distributions discussed in the preceding paragraph. In Fig. 14, the airspeed was 93 ft/s and the corresponding lift coefficient was 0.59. For the "high" porosity

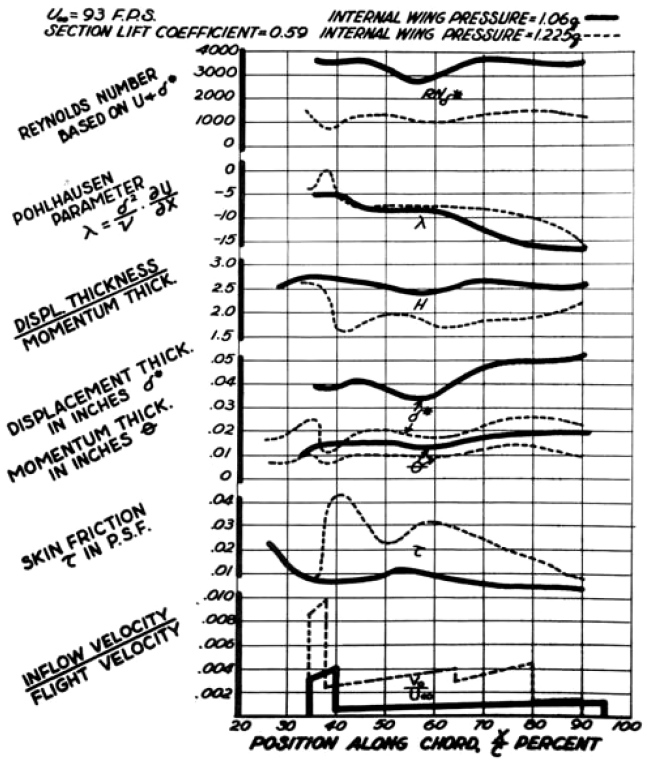

Fig. 14 Boundary-layer property variations for Carmichael's first and second porosity distributions for a flight speed of 93 ft/s (Fig. 4 in [9]).

distribution (corresponding to the dashed lines in the figure), the minimum suction pressure required was $1.225q$. For the "low" porosity distribution (corresponding to the solid lines in the figure), the required minimum suction pressure was $1.06q$. In Fig. 15, the airspeed was 123 ft/s and the corresponding lift coefficient was 0.34. The minimum suction pressure required for the high-porosity

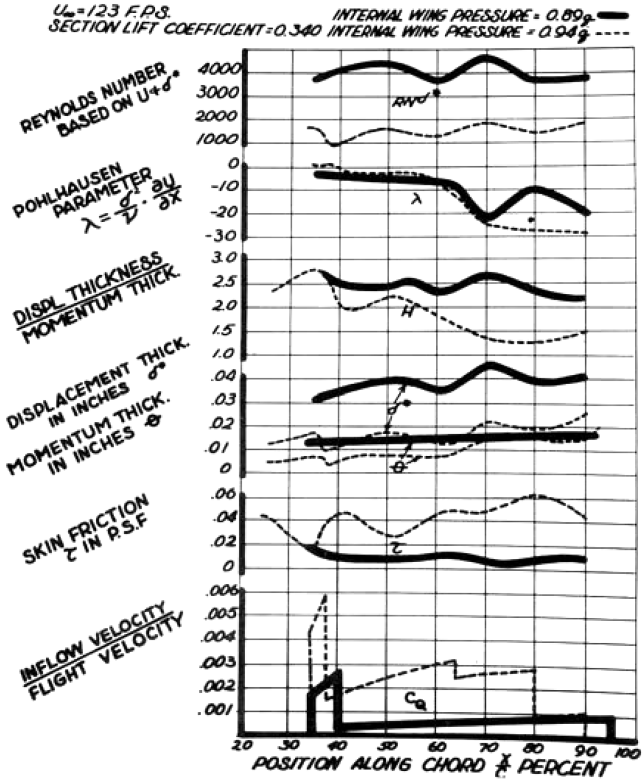

Fig. 15 Boundary-layer property variations for Carmichael's first and second porosity distributions for a flight speed of 123 ft/s (Fig. 5 in [9]).

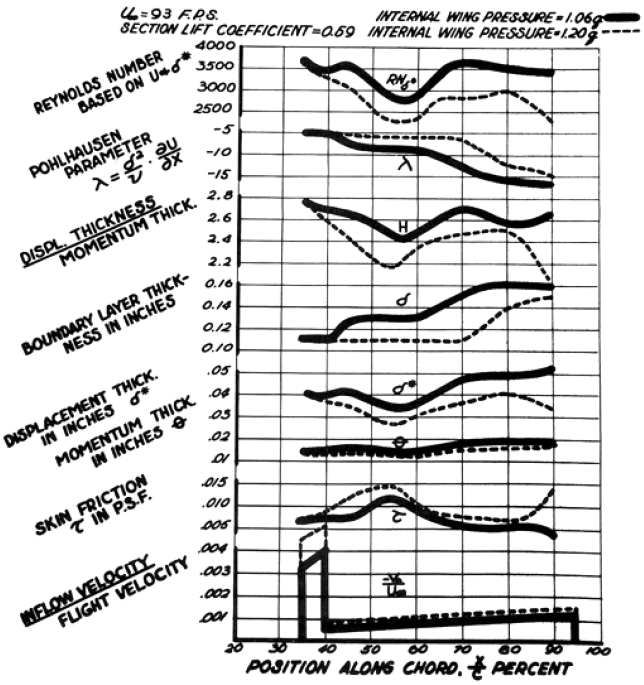

Fig. 16 Boundary-layer property variations for Carmichael's second porosity distribution for two different internal suction pressures (Fig. 6 in [9]).

distribution was $0.94q$, and the required minimum suction pressure for the low-porosity distribution was $0.89q$. What Carmichael [9,22] noted from these results was that the wall shear remained low and the shape factor H remained high for the lower values of the internal suction pressures and corresponding lower porosity distributions. The boundary layer reached a value of Pohlhausen's parameter of -17, yet the boundary layer remained attached and laminar. At the higher speed, the results shown in Fig. 15 show that the boundary layer reached a Reynolds number based on displacement thickness of 4600, which was the highest value that had been obtained to date for a suction-stabilized boundary layer.

Figure 16 demonstrates the effects of two different internal suction pressures for the same porosity distribution. The porosity distribution is the low-porosity from the previous two figures, and the suction pressures are $1.06q$ (solid lines) and $1.20q$ (dashed lines). The high value of the internal suction pressure was the maximum that could be applied while maintaining complete stabilization (full-chord laminar flow). The larger value of the suction pressure caused the boundary layer to be thinner and reduced the value of H.

Figures 14–16 show that the application of suction causes a reduction in momentum thickness at the trailing edge that would correspond to a decrease in the external drag of the airfoil section. To verify this, the following result of Squire and Young [23,24] was used to compute the external drag of the section:

$$C_D = \frac{2\theta}{c}\left(\frac{U}{U_\infty}\right)^{\frac{H+5}{2}} \tag{1}$$

In this formula, θ is the momentum thickness, H is the shape factor, c is the airfoil chord, U is the local boundary-layer edge velocity, and U_∞ is the freestream velocity. In the original formula by Squire and Young, all quantities were evaluated at the trailing edge of the body. In the work by Carmichael [9,22], each of these quantities was evaluated at the 90% chord location ($x/c = 0.9$) for each value of the internal suction pressure studied for a flight speed of 93 ft/s. The cost of the suction was computed as an equivalent suction drag coefficient. It was assumed that the air sucked into the wing at a pressure Δp below the freestream was eventually raised to the freestream pressure. The corresponding suction drag coefficient was therefore

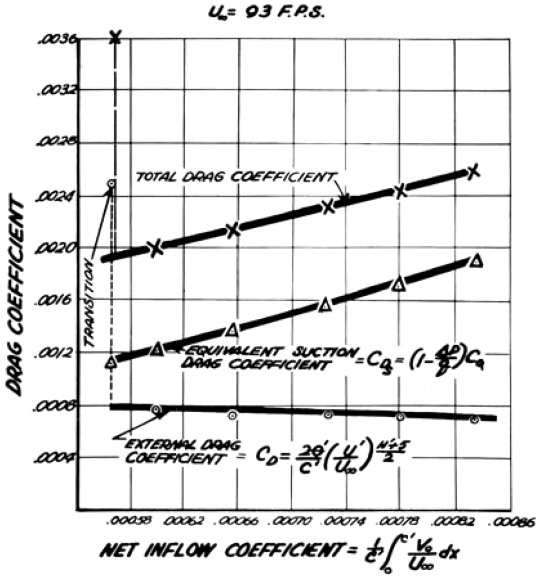

Fig. 17 External, suction, and total drag coefficients as functions of suction flow coefficient for a flight speed of 93 ft/s (Fig. 7 in [9]).

$$C_{Ds} = (1 - \Delta p/q)C_Q \tag{2}$$

where C_Q is the corresponding suction coefficient and represents the rate at which the air was sucked into the wing. The results of these investigations are shown in Fig. 17 (Fig. 7 from [9]). This figure shows the gradual reduction in the external drag coefficient with increased suction, due primarily to the decrease of the momentum thickness of the boundary layer. However, as the suction coefficient goes up, C_{Ds} goes up faster than the external drag coefficient goes down, and so the net drag coefficient goes up. This figure does illustrate the benefit of applying as little suction as possible. As Carmichael pointed out in the report, it was not possible to achieve an absolute minimum in the overall drag because the boundary layer transitioned to turbulent, yielding the points at the far left of the figure. However, there was an overall reduction in drag for this airfoil as the result of the application of suction. For this airfoil, at a chord of $Re = 3 \times 10^6$, the drag coefficient of the original rough airfoil was 0.0105, of the smooth airfoil, 0.0075, and of the smooth airfoil with suction, 0.004, a reduction of approximately 53% over the smooth impervious airfoil value. Carmichael stated that further reductions in drag should be possible with further iterations on the porosity distribution.

The determination of the optimum suction distribution was the subject of the next report by Carmichael, in which the results of 19 different porosity distributions were reported [8] (this summary by Carmichael includes results for some distributions reported in previous studies). The tests continued to make use of the TG-3A glider with an NACA 4416 airfoil section. As before, the portion of the wing ahead of the trailing edge of the spar at $x/c = 0.345$ was impervious. The first six distributions described in the report by Carmichael [8] contain the distributions in the reports previously discussed [3,6,9]. For the first four distributions studied, the porosity extended to $0.9c$. For the next two distributions, the porosity extended to $0.95c$, and to c for the remainder of the distributions examined. Because of the variations in the extent of the porosity, the actual area of the porous region in each case was used in the definition of the suction coefficient and the equivalent suction drag coefficient. The suction drag coefficients so defined must be distinguished from overall suction drag coefficients used in performance calculations (the suction drag coefficients reported must be multiplied by the ratio of porous to reference areas to be added to wake drag coefficients to obtain total drag coefficients). In a number of cases, full stabilization was not achieved. The distributions were thus compared using a figure of merit, which was the ratio of the stabilized area to porous area divided by the equivalent drag coefficient for the internal suction, as defined in Eq. (2):

$$\text{FOM} = \frac{S_{\text{stabilized}}/S_{\text{porous}}}{C_{Ds}} \tag{3}$$

As noted, Carmichael began by providing some details concerning the results published in previous reports [3,6] and discussed herein. He then reported on further empirical studies aimed at determining the optimum suction distribution for maximum stabilization of the boundary layer on the glider wing. The final design arrived at in this manner used 0.018-in-diam holes spaced 0.125 in. apart for $0.345 < x/c < 0.40$ and then 0.012-in-diam holes spaced 0.25 in. apart for $0.40 < x/c < 0.95$. The resulting flow had a FOM of over 200 and was reported to be the best performance of any suction distribution to that time. It was the results for this distribution that were reported by Carmichael in [9]. It was noted by Carmichael that the shape factor H for this particular suction distribution had a value close to 2.6, the value for the Blasius boundary layer, over most of the airfoil section. This prompted Carmichael to speculate that the concept of momentum conservation might be applied to create a boundary layer that would be less susceptible to transition.

B. Theory of Momentum Conservation

The concept of applying the principle of momentum conservation to create boundary layers with desired characteristics had been developed by Raspet [25]. It was based on the momentum equation as adapted by Prandtl:

$$\tau_w = \rho U v_w + \rho U \frac{dU}{dx}(\delta^* + 2\theta) + \rho U^2 \frac{d\theta}{dx} \tag{4}$$

In this equation, τ_w is the shear stress at the wall, ρ is the fluid density, U is the velocity at the edge of the boundary layer, v_w is the wall suction velocity, δ^* is the boundary-layer displacement thickness, θ is the boundary-layer momentum thickness, and x is the streamwise coordinate measured along the wall. This equation may be rewritten as

$$\frac{d\theta}{dx} = \frac{c_f}{2} - (2 + H)\frac{\theta}{U}\frac{dU}{dx} - C_Q \tag{5}$$

In this equation, c_f is the skin friction coefficient, H is the shape factor, and $C_Q = v_w/U$ is the local flow coefficient. If the parameter K is defined as

$$K \equiv \frac{\tau_w \delta^*}{\mu U} \tag{6}$$

then for the Blasius boundary layer, $K = 0.57$, and for the asymptotic boundary layer with suction, $K = 1.00$. With the parameter β defined as

$$\beta = \left(\frac{2}{H} + 1\right)K \tag{7}$$

Eq. (5) may be rewritten as

$$C_Q = \frac{\tau_w}{\rho U^2} - \beta\frac{\mu}{\tau_w}\frac{dU}{dx} - \frac{d\theta}{dx} \tag{8}$$

The boundary-layer development may be "programmed" by particular choices of $d\theta/dx$. One particular example is the case where $d\theta/dx = 0$ so that the momentum thickness is constant along the chord. The value of the wall shear stress that yields a minimum value of C_Q is then

$$\tau_w = \sqrt{\beta\mu\rho U^2\left(-\frac{dU}{dx}\right)} \Rightarrow v_w = 2\sqrt{\beta}\sqrt{\nu\left(-\frac{dU}{dx}\right)} \tag{9}$$

This result may be used to compute the suction required for conservation of momentum (as defined by the condition of constant momentum thickness) in the boundary layer. The resulting distribution for conservation of momentum with H and K equal to the Blasius values is $v_w = 2.00[\nu(-dU/dx)]^{1/2}$, and

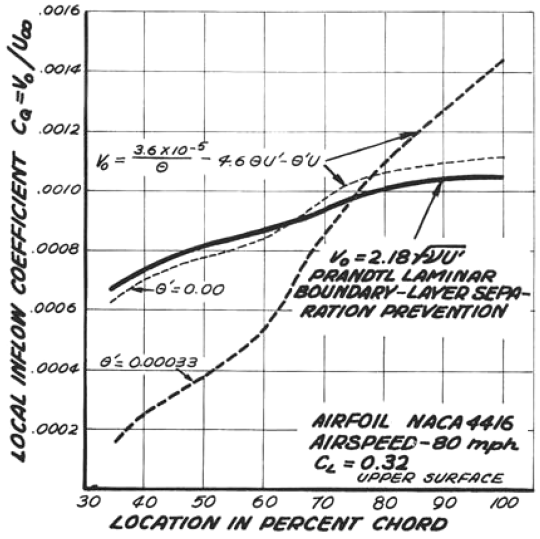

Fig. 18 Comparison of required suction flow distributions for NACA 4416 airfoil at $C_L = 0.32$ (Fig. 2 in [25]).

$v_w = 2.828[\nu(-dU/dx)]^{1/2}$ with the values of H and K for the asymptotic boundary layer with suction. According to Raspet, Prandtl computed a value of $v_w = 2.18[\nu(-dU/dx)]^{1/2}$ for the critical condition of laminar separation. Raspet concluded that Prandtl's condition must have been slightly excessive in its suction requirements, because it exceeded that required for momentum conservation in the Blasius boundary layer.

Using the definition of K from Eq. (6), Eq. (5) may be rewritten in the form

$$v_w = \frac{\nu K}{H\theta} - (2+H)\theta\frac{dU}{dx} - U\frac{d\theta}{dx} \tag{10}$$

By assuming different values of (constant) K and H, the wall suction velocity required for a particular desired boundary-layer development may be computed, as long as the momentum thickness at the beginning of the distribution is known. For the boundary layer in which momentum is conserved ($d\theta/dx = 0$), using the values of K and H for the Blasius profile, this equation reduces to

$$v_w = \frac{0.23\nu}{\theta} - 4.6\theta\frac{dU}{dx} \tag{11}$$

(It should be noted that this equation uses the value of 0.23 as reported by Raspet [25], although it is not completely clear where this value came from, because with $K = 0.57$ and $H = 2.6$ for the Blasius profile, $K/H = 0.219$).

The required suction velocity distributions were computed for a NACA 4416 airfoil section at a lift coefficient of 0.32 for three different cases, one for the Prandtl separation condition, one for momentum conservation, and one allowing a gradual growth of the momentum thickness of the boundary layer, $d\theta/dx = 0.00033$. These are compared in Fig. 18 (Fig. 2 in [25]). Prandtl's distribution and the momentum conservation distribution are seen to be quite close to each other. Raspet also compared the theoretical suction distribution required for momentum conservation to the distribution obtained by Carmichael [9] for boundary-layer stabilization with the highest FOM, and noted that the empirically determined suction distribution followed fairly closely the distribution that would have been required for momentum conservation.

Raspet went on to examine the experimental works of other authors to verify his principles of momentum conservation in the boundary layer. Based on these examinations, Raspet concluded that the use of a constant value of K was justified, that it was possible to determine a suction distribution such that a constant value of the shape parameter $H = 2.6$ could be achieved, and that suction distributions close to the optimum as computed from the momentum integral equation were sufficient for retaining Blasius-like profiles. Raspet then examined experimental results for boundary-layer stabilization, and concluded that it was sufficient for stabilization to apply just enough suction to achieve Blasius-type profiles. The resulting profiles were thicker and therefore less susceptible to effects of surface roughness than asymptotic suction profiles, which would also require higher levels of suction and therefore incur a higher drag cost penalty. Raspet's goal in this paper was to demonstrate that extraordinarily high levels of suction were *not* required to stabilize a boundary layer.

C. Application of Momentum Conservation Theory

In order for Carmichael [8] to make use of Raspet's momentum conservation theory, he had to determine the distribution over the wing of the pressure difference Δp between the inside and the outside of the wing at a given flight condition, and the dependence of the suction flow velocity v_w through each hole as a function of the pressure difference Δp at a given hole, and the hole diameter D. The "flying" static pressure probe was used to determine the external pressure distribution over the wing at a given flight condition. A series of tests [8] showed that the volumetric flow rate Q per unit distance was proportional to $\Delta p^{1/2}$ except at small values of Δp. The quantity Q varied approximately with the hole diameter squared, although it was noted that for a spanwise hole spacing of 20 holes/in., Q was proportional to $D^{1.8}$ and for a spacing of 10 holes/in., Q was proportional to $D^{2.3}$ (it should be noted that only two hole diameters, $D = 0.018$ in. and $D = 0.12$ in., were tested).

Using this information, Carmichael [8] attempted to stabilize the boundary layer with a suction velocity distribution designed initially to produce a slight growth in the momentum thickness, $d\theta/dx = 0.00045$, at a flight speed of 60 mph. Various attempts to do this were unsuccessful or only moderately successful. Those that did succeed in achieving a significant amount of flow stabilization required a large amount of porosity immediately behind the spar. To find out why this was happening, the wing section was made

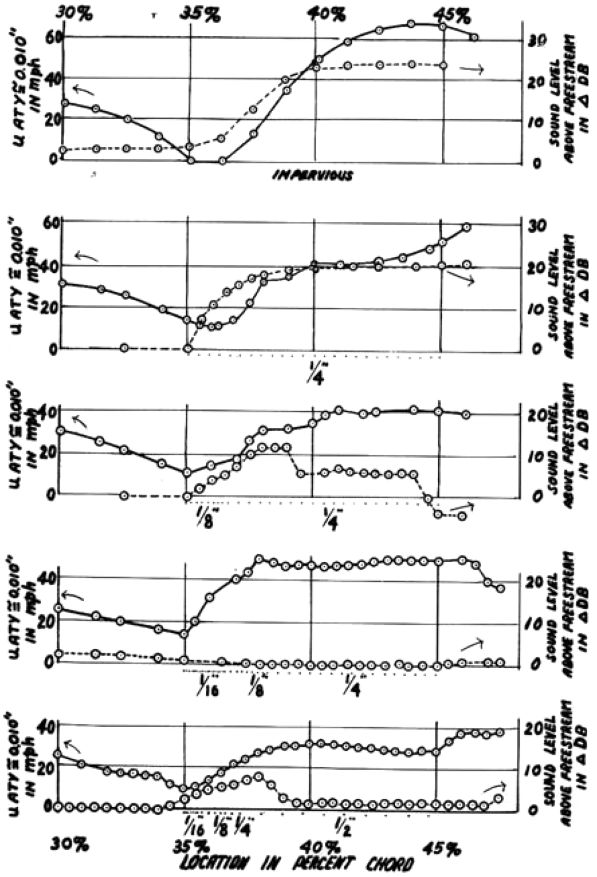

Fig. 19 Determination of porosity distribution required to prevent separation behind spar of TG-3A glider wing (Fig. 11 in [8]).

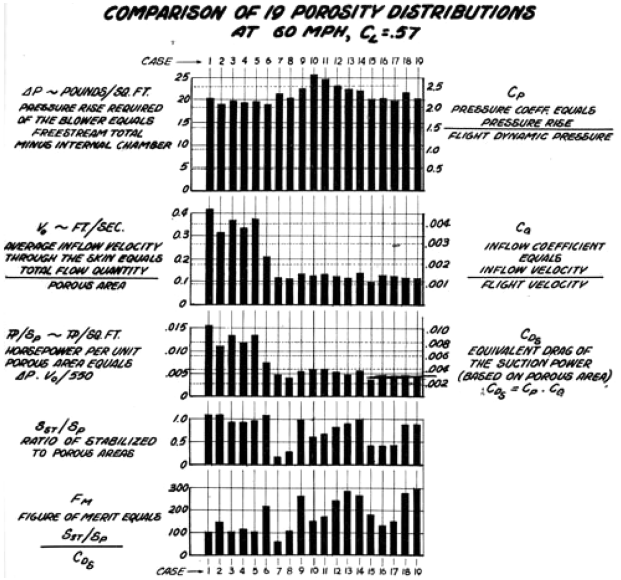

Fig. 20 Results for all porosity distributions for the glider at 60 mph and $C_L = 0.57$ (Fig. 2 in [8]).

impervious for $0.345 < x/c < 0.40$ and boundary-layer surveys were conducted. These surveys showed that at all flight speeds tested (even the highest flight speed of 100 mph, corresponding to a chord in excess of $Re = 4 \times 10^6$), a laminar separation was occurring near $x/c = 0.33$, followed by a turbulent reattachment near $x/c = 0.40$. At the highest airspeed, reversed flow occurred at $x/c = 0.38$. The higher porosity in the region just aft of the spar in some of the distributions studied was the reason why those distributions produced better performance. Using this information, the porosity distribution between $x/c = 0.345$ and $x/c = 0.40$ was gradually increased using 0.018-in-diam holes. Figure 19 (Fig. 11 in [8]) shows the process by which the optimum porosity distribution was obtained. The solid curve in each pair of curves is the velocity at $y = 0.010$ in. and was used in the manner of a Preston tube to indicate surface shear stress. The dashed curve is the sound level measured with the electronic stethoscope discussed earlier. The top pair of curves are for the impervious section and show the wall shear stress going to zero, followed by a rapid increase which tracks the increase in sound level. This is behavior typical of a laminar

Fig. 22 Schweitzer TG-3A used for boundary-layer separation studies.

separation followed by a turbulent reattachment. The next pair of curves shows the results for the initial porosity distribution. Separation was apparently prevented, because the wall shear did not go to zero, but transition still occurred, as evidenced by the rise in sound level and in wall shear stress. The next two pairs of curves show gradual improvement, with no apparent transition, as evidenced by the sound level curve in the next-to-last pair of curves. However, for this application of suction, the wall shear stress reached a very high level, caused by the excessive thinning of the boundary layer due to excessive suction. The final distribution, shown in the bottom pair of curves, achieved a nominally stable boundary layer with an acceptable rise in the wall shear stress. This distribution immediately aft of the spar was then used for all subsequent porosity distribution studies.

Two more porosity distributions were tested. The next-to-last distribution provided good stabilization at airspeeds of 60 and 70 mph, but less satisfactory results at 80 mph. This distribution was smoothed out using the momentum equation, and the FOM at 80 mph was improved substantially. Figure 20 summarizes the results for all of the distributions tested at an airspeed of 60 mph. It can be seen in Fig. 20 that 100% stabilization was achieved for several of the distributions tested ($S_{\text{stabilized}}/S_{\text{porous}} = 1$ or greater) at 60 mph. A similar figure in the report shows that 100% stabilization was not achieved for any of the porosity distributions at 80 mph. However, the FOM was substantially higher for the final distribution tested than any of the previous distributions. The FOM values for the last distribution tested were 3, 2.6, and 3.75 times greater than the values for the original distribution at airspeeds of 60, 70, and 80 mph, respectively.

Carmichael addressed one other issue during these studies: the fact that full stabilization could be maintained only over a narrow range of internal suction pressure values. This issue had been noted in the earlier studies. The transition locations for the final porosity distribution are shown in Fig. 21 (Fig. 8 from [8]) as a function of the

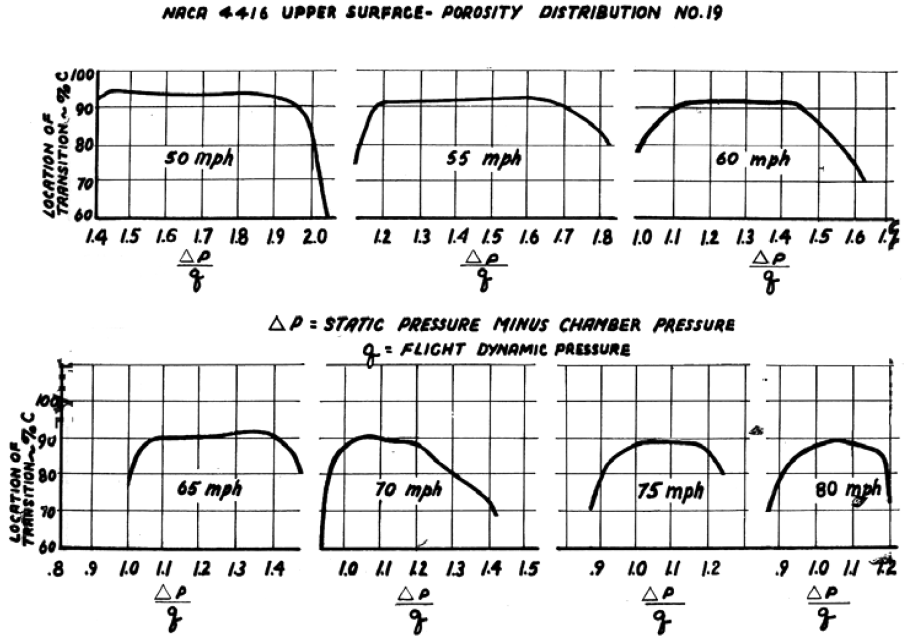

Fig. 21 Transition locations for the Carmichael's final porosity distribution as a function of internal suction pressure and airspeed (Fig. 8 in [8]).

ratio of internal suction pressure Δp to the dynamic pressure q for each of the airspeeds tested. These figures indicated the small range of internal pressures over which full stabilization could be maintained. This difficulty was attributed to the limitation of a single suction compartment and the corresponding high local suction values at high speeds that were thought to destabilize the boundary layer.

IV. Boundary-Layer Separation Studies

It will be recalled that the boundary-layer transition studies just discussed were prompted by a desire to create a laminar boundary layer that would more closely match the inviscid flow conditions assumed by Smith [14], who had predicted an improvement in airfoil lift coefficient through the use of trailing-edge suction. An increase in maximum lift coefficient produced by an airfoil was a significant goal in Raspet's work, because such an increase would lead to improvements in glider performance and also in short takeoff and landing (STOL) applications. As the boundary-layer transition experiments were completed in 1953 and 1954, the focus began to shift to the prevention of boundary-layer separation through the use of distributed suction.

As Carmichael had taken the lead in the boundary-layer transition studies, Joseph Cornish III, a graduate student working under Raspet, led most of the boundary-layer separation studies. In the first study [10] of the prevention of separation of a *turbulent* boundary layer, Cornish also used a modified TG-3A glider with a wing area of 237 ft^2, an aspect ratio AR = 12.3, and a wing loading of 5.2 lb/ft^2. This glider is shown in Fig. 22. During the course of the studies to be discussed, the compartment ahead of the spar was made into a suction compartment, so that two suction motors were required. The suction motor for the rear portion of the wing may be seen in the wing root of the TG-3A in Fig. 22. Figure 23 shows schematically the layout of the two suction compartments within the wing.

The maximum lift coefficient that could be obtained from the glider with no boundary-layer control applied was 1.38 at an airspeed of 38.5 mph. Distributed suction was then applied to the areas of the wing shown in the top diagram of Fig. 24 (Fig. 4 in [10]). In the shaded region, 50 rows of 0.018-in-diam holes were punched with a spanwise spacing of 20 holes per inch. The first row was located at $x/c = 0.35$ and the chordwise spacing was determined by the wall velocity distribution necessary to maintain a constant momentum thickness for the pressure distribution on the wing at an airspeed of 40 mph. The momentum thickness on the impervious portion of the wing at $x/c = 0.35$ was used as the initial momentum thickness for the wall velocity computations. With this application of porosity, the

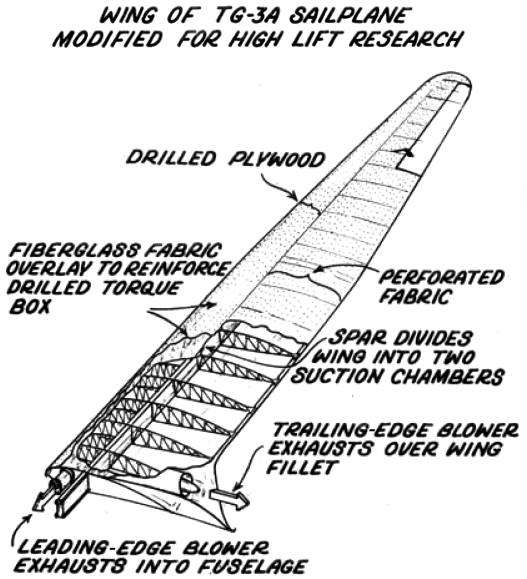

Fig. 23 Schematic of interior of TG-3A wing showing two compartments and two suction motors (Fig. 2 in [27]).

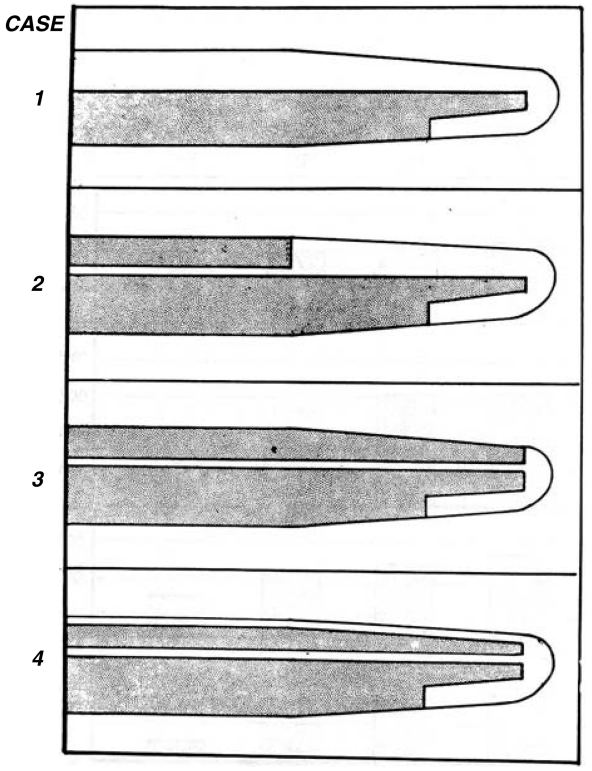

Fig. 24 Porosity distributions used on TG-3A wing during initial separation prevention tests (Fig. 4 in [10]).

maximum lift coefficient of the glider was increased to 1.61 at an airspeed of 35.5 mph. The required suction coefficient C_Q was 0.00149. However, when boundary-layer measurements were made on the wing at this condition, it was determined that the applied suction was not creating a boundary layer with a constant momentum thickness.

The second diagram in Fig. 24 shows the region of perforations applied ahead of the $x/c = 0.3$ location. This porosity was added to reduce the momentum thickness ahead of $x/c = 0.3$, because the momentum thickness at that point without suction had become too large for the porosity aft of $x/c = 0.3$ to reduce momentum losses. These perforations required drilling through the plywood leading edge of the wing, so that the leading edge/spar cap became a suction compartment, as discussed. The holes were spaced 10 per inch in the spanwise direction. The chordwise spacing was determined using the known pressure distribution and the momentum equation as discussed previously. The additional suction ahead of $x/c = 0.3$ increased the maximum lift coefficient to 1.98 at an airspeed of 32 mph. The required suction coefficient was $C_Q = 0.00264$.

In spite of the additional suction ahead of $x/c = 0.3$, the momentum thickness at $x/c = 0.35$ was still too large for the criterion used to design the porosity distribution aft of $x/c = 0.35$. Rather than adding more porosity at the leading edge, the decision was made to modify the aft porosity distribution. The third diagram in Fig. 24 shows the additional perforated regions. Fourteen rows of holes were punched between existing rows of holes aft of $x/c = 0.35$. Behind these 14 additional rows, 7 rows were added alternating between existing rows. The extra holes increased the

Table 1 Comparison of results for porosity distributions shown in Fig. 27

Case	1	2	3	4
ΔC_L	0.23	0.60	0.82	0.90
C_Q	0.00149	0.00264	0.00316	0.00316
$\Delta C_L/C_Q$	154	227	259	285
$C_{Ps} \times C_Q$	0.00545	0.0103	0.0180	0.0188

suction coefficient C_Q to 0.00316 and the maximum lift coefficient to 2.2 at an airspeed of 30.2 mph. Additional studies of the boundary layer near the leading edge (to be discussed next) indicated that the holes in the area $0.015 < x/c < 0.05$ should be closed, yielding the porosity distribution shown in the last diagram of Fig. 24. With this porosity distribution, the maximum lift coefficient was 2.28 at an airspeed of 29.8 mph and a suction coefficient $C_Q = 0.00316$. The results for the four different porosity distributions are shown in Table 1. The increment in lift coefficient ΔC_L is the increase in lift coefficient over the maximum lift coefficient of 1.38, as noted before. In this table, the figure of merit is the ratio of the change in lift coefficient divided by the suction coefficient, or FOM $= \Delta C_L / C_Q$. The last row in this table is equivalent to the suction drag coefficient defined by Eq. (2). As can be seen in Table 1, the fourth porosity distribution had the highest figure of merit with FOM = 285.

The initial studies on the boundary layer at the leading edge of the wing showed that a laminar separation bubble existed in the vicinity of $x/c = 0.04$. It had been assumed that extending the perforations to the leading edge would eliminate this problem. However, the additional studies mentioned in the preceding paragraph showed that the application of suction near the leading edge made the bubble worse. This is illustrated in Figs. 25 and 26 (the first two parts of Fig. 7 in [10]), which are plots of constant velocity contours in the boundary layer. Figure 25 shows the small bubble region for $x/c < 0.05$ with no suction applied. Figure 26 shows the dramatic increase in the size of the bubble region with suction applied, counter to what had been expected. Figure 27 (Fig. 8 in [10]) shows the impact on the momentum thickness at $x/c = 0.35$ of the initial location of application of suction. This figure shows that the momentum thickness at $x/c = 0.35$ decreased rapidly when the initial application of suction was moved from $x/c = 0.015$ to $x/c = 0.05$. Cornish noted that these results were consistent with a conclusion reported by McCullogh and Gault [26] which stated that the application of suction should begin just downstream of the separation point on the impervious section. It was Cornish's study of the boundary layer at the leading edge that led to the decision to close the perforations in the region $0.015 < x/c < 0.05$ previously mentioned.

Figure 28 (Fig. 9 in [10]) shows the effects of adding suction to the TG-3A wing. The wing on the TG-3A had an NACA 4416 section,

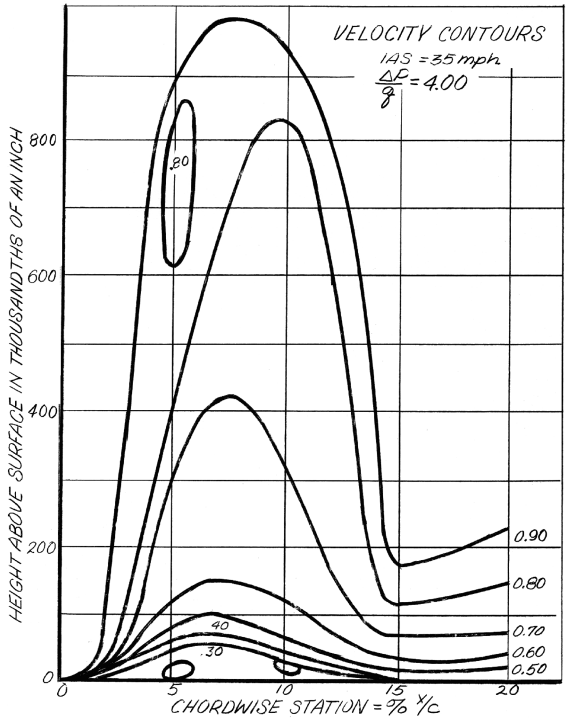

Fig. 26 Boundary-layer velocity contours for TG-3A wing with moderate suction (Fig. 7b in [10]).

which is a relatively thick airfoil. Figure 28 shows the apparent increase in lift curve slope with the application of suction, indicating that suction was overcoming trailing-edge stall, common on thick airfoils. Figure 28 also shows the detrimental effects of wing porosity when the suction is turned off. The wing performance was degraded significantly.

At approximately the same time as the initiation of the separation prevention studies, Cornish performed a relatively extensive study of boundary-layer measurement techniques [5]. This study appears to

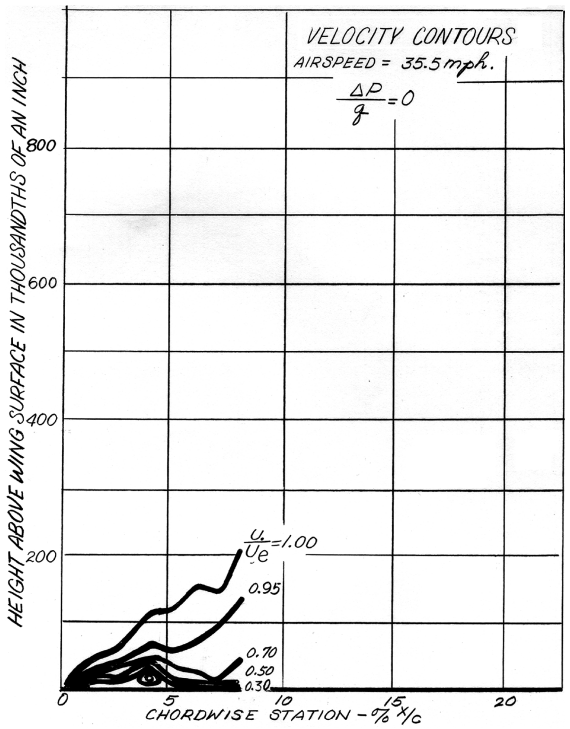

Fig. 25 Boundary-layer velocity contours for TG-3A wing with no suction (Fig. 7a in [10]).

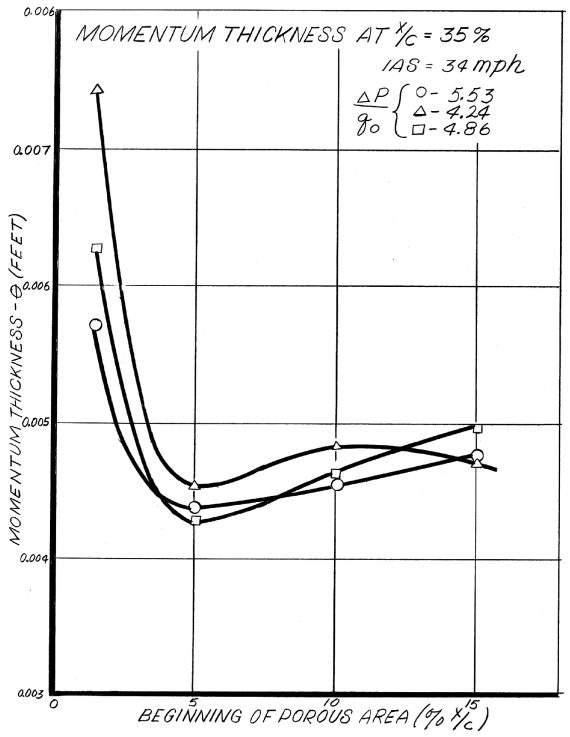

Fig. 27 Effect of initial perforation location on momentum thickness at $x/c = 0.35$ (Fig. 8 in [10]).

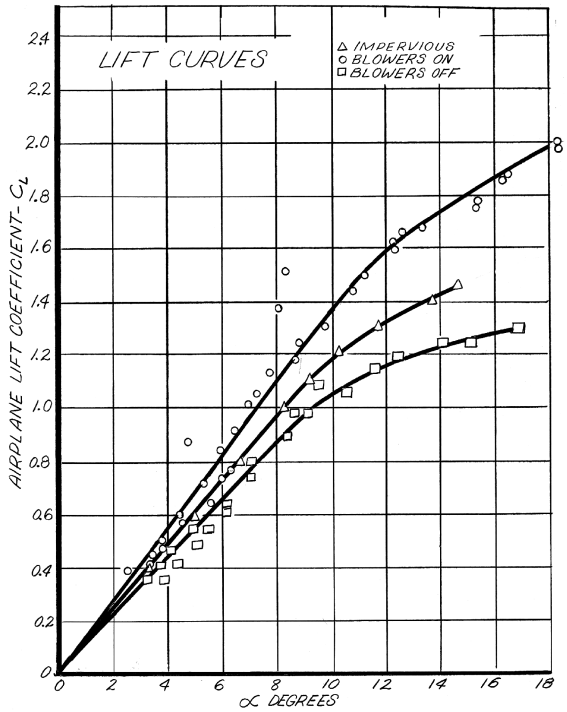

Fig. 28 Lift curves for TG-3A glider showing effects of suction boundary-layer control (Fig. 9 in [10]).

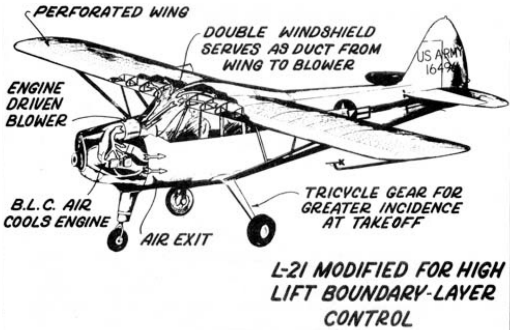

Fig. 30 Schematic of application of suction boundary-layer control to L-21 (Fig. 3 in [27]).

have been performed to ensure that the measurement methods to be used in the separation studies were valid and yielded reasonably accurate results when applied in flight tests. The boundary-layer mouse (Fig. 5) and the surface shear stress meter (Fig. 6) were used to make detailed studies of the boundary layer on the TG-3A glider with an impervious wing. The distribution of displacement thickness, momentum thickness, and shape factor over the wing were documented at several different speeds. The boundary-layer profiles were used with various methods for calculating the wall shear stress and these were compared with the measured values. The use of Clauser's method with the boundary-layer velocity profiles gave the best agreement to the wall shear stress values computed using the surface shear meter and Preston's calibration curve. Transition locations determined using the surface shear meter and the stethoscope were also in good agreement.

Attention was then turned to the application of boundary-layer control to a powered aircraft [27,28], an L-21, which was the military version of the Piper PA-18 "Super Cub." The L-21 had a wing span of 35 ft, a wing area of 178 ft^2, a weight of 1500 lb, and was powered by a Lycoming 125 hp engine driving a fixed-pitch propeller with a diameter of 72 in. The initial study aimed at applying boundary-layer control to the aircraft in a takeoff and minimum flying speed configuration, with landing and cruise conditions considered secondary issues. A photograph of the airplane is shown in Fig. 29 and a schematic illustration of the application of the suction boundary-layer control is shown in Fig. 30. A belt-driven blower was mounted above the engine, and the ducting from the wing to the blower was provided by a double windshield. The air pulled from the inside of the wing by the blower motor passed through the gap between the two windshields. To remove the obstruction to the suction flow inside the wing, the wing fuel tanks were removed and replaced with a tank behind the pilot's seat. The flaps were also sealed and ducting provided from the flap interiors to the wing interior so that suction could be applied to the flaps as well. Because the flaps were formed from aluminum, the fabric puncher shown in Fig. 9 was insufficient to perforate the flaps, so an automatic hole driller (Fig. 31) was built. This device was powered by a small air turbine and could drill 0.020 in. holes in 0.030-in. aluminum skin at the rate of five per second. The original conventional ("tail-dragger") landing gear was replaced by a tricycle landing gear so that increased angles of attack could be achieved on takeoff when the aircraft rotated.

This first test of the application of boundary-layer control to a powered aircraft was intended primarily as an engineering test to prove the feasibility of the concept. Optimal boundary-layer control was not the primary goal. Rather, a set of measurements of the boundary layer on the aircraft without control would be made and a suction distribution based on those measurements would be designed, yielding the total amount of suction required. The pressure losses in the ducting would be estimated, and thus the pressure and flow requirements of the pump would be obtained. The system would then be built and evaluated based on the lift gained for the additional power expended.

The initial suction distribution applied to the L-21 was designed using the momentum integral equation [Eq. (5)], with the value of $d\theta/dx$ set at 0.002, which according to Raspet et al. [27] was half the value of the rate of momentum thickness growth for the impervious wing. On the L-21, the metal leading edge extended to $x/c = 0.15$, and the wing was covered with fabric aft of that point. It was decided to begin the perforations at that point. Flight tests of the airplane at 38 mph were conducted to determine the velocity distribution over the wing and the boundary-layer properties at $x/c = 0.15$. It was noted that at this speed, turbulent separation occurred in the range $0.80 < x/c < 0.85$, and that the flap was completely stalled at all settings except $\delta_f = 0$ deg. The velocity profile at $x/c = 0.15$ yielded the value of the momentum thickness, which was necessary to begin the computation of the suction distribution from that point

Fig. 29 L-21 observation aircraft used for boundary-layer control studies.

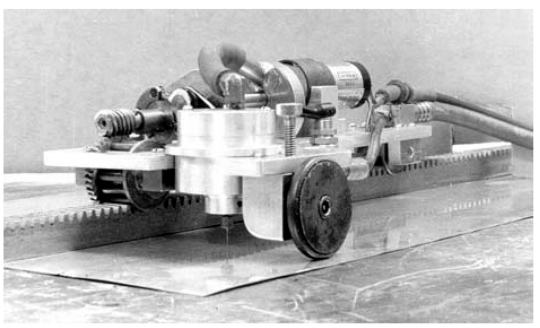

Fig. 31 Automatic hole drilling device.

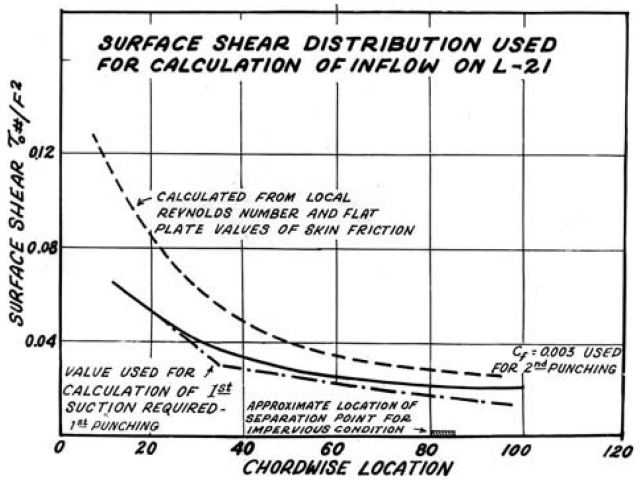

Fig. 32 Surface shear stress distribution assumed in design of porosity distributions applied to L-21 (Fig. 5 in [27]).

using Eq. (5). It was assumed that the shape factor H would remain constant at its turbulent value of 1.45 under the application of suction. The distribution of surface shear stress assumed for the initial porosity distribution is shown in Fig. 32 (Fig. 5 in [27]). The diameter of the holes was 0.030 in. In theory, the highest allowable internal suction pressure would be determined by the local static pressure at $x/c = 0.15$, which was the location in the perforated region of the lowest external pressure on the wing, to prevent outflow from the wing. In practice, it was necessary to make the internal pressure considerably lower than the lowest external pressure, to avoid extremely small row spacings that would result from using the minimum external pressure criterion. The initial internal pressure was chosen such that the resulting porosity distribution allowed a chordwise spacing of at least 0.1 in. between hole rows.

When the initial suction distribution was tested in flight, it was discovered that the flow coefficient of the holes was less than expected, and that the internal suction pressure developed by the pump was not as low as had been computed. Two more distributions were developed, taking into account the lower suction pressure and using information from a concurrent glider test. The third suction distribution resulted in an increment in lift coefficient $\Delta C_L = 1.82$

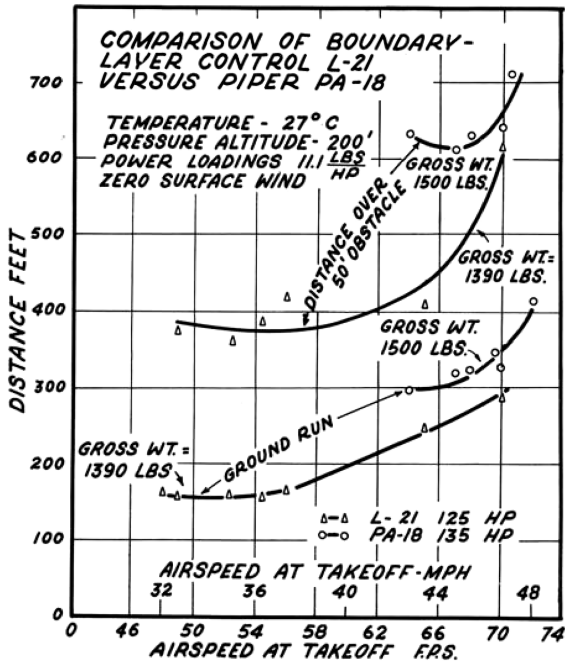

Fig. 33 Comparison of takeoff distances for L-21 with boundary-layer control and PA-18 without boundary-layer control (Fig. 10 in [27]).

Table 2 Comparison of maximum lift coefficients obtained on aircraft without and with suction

	PA-18 no boundary-layer control		Army L-21 boundary-layer control	
Flap setting	Power off	Full power on	Power off	Full power on
0	1.3	1.6	2.6	2.5
1/3	n/a	n/a	2.8	3.2
1/2	1.4	2.0	2.8	3.0
Full	1.55	2.16	3.0	4.0

and a stall speed of 28 mph at a flow coefficient $C_Q = 0.00605$. The amplification was $\Delta C_L/C_Q = 301$ and the suction power required was 2.08 hp. The overall lift coefficient obtained using this suction distribution was $C_L = 3.98$. At this maximum lift coefficient, the stall behavior of the aircraft indicated that stall was resulting from laminar separation near the leading edge. This type of separation had been noted as the limiting factor on the maximum angle of attack that could be obtained with sailplanes. No further efforts were made to influence the behavior of the turbulent boundary layer.

In addition to the low-speed cruise values just discussed, the effects of boundary-layer suction on the takeoff of the L-21 were also examined. The total distance required to clear a 50 ft obstacle was measured for the L-21 with boundary-layer control and a Piper PA-18 without suction. The PA-18 had a 135 hp engine as compared with the 125 hp engine of the L-21, so the weight of the PA-18 was increased so that the power loading (weight per horsepower) would have the same value of 11.1 lb/hp for the two aircraft. The resulting test weight was 1390 lb for the L-21 and 1500 lb for the PA-18. The ground run and total takeoff distance for the two aircraft are compared in Fig. 33 (Fig. 10 in [27]). A reduction in the total takeoff distance of 42% for the L-21 with boundary-layer control can be seen in the figure. It was noted that the climbout angle at the low takeoff speeds was not as large as the maximum climbout angle that could be achieved at higher speeds, implying that the reduction in overall takeoff distance was less than what might be achieved with a more efficient boundary-layer control mechanism.

The maximum lift coefficients that could be obtained for the two different aircraft are shown in Table 2 (Table 1 in [27]). Note that the increment in lift coefficient for full flaps with boundary-layer control and full power on was 1.0, where the increment for full flaps without boundary-layer control and full power on was 0.6. Raspet et al. [27] concluded that the flap with suction was turning the slipstream of the propeller downward and thus creating additional lift.

Boundary-layer control was applied to a second powered aircraft, an L-19 (shown in Fig. 34). According to Cornish [29], the unmodified L-19 could achieve a maximum lift coefficient of 3.36 with full flaps and full power, and a maximum lift coefficient of 2.23 with full flaps and power set to idle. With the addition of distributed suction, the idle-power maximum lift coefficient was unchanged, but the full-power maximum lift coefficient was increased to 3.93. It was noted that the aircraft could not be stalled in the idle-power condition because the moment that could be generated by the tail was insufficient. Studies of the wake of the wing revealed a "notch" in the dynamic pressure of the wake passing over the tail, even with the flow attached to the flap because of the suction. The region of lower dynamic pressure was passing over the tail, leading to a decrease in

Fig. 34 L-19 observation aircraft with boundary-layer control.

the aerodynamic forces that could be produced by the horizontal stabilizer. The flap geometry was modified to eliminate the gap between the flap and the wing, creating what Cornish termed a camber-changing flap. The wing leading edge was also modified by increasing the leading-edge radius and "drooping" the leading edge (to be discussed later). With the suction boundary-layer control and the modifications to the flap and wing leading-edge geometries, the maximum lift coefficient for full flaps and full power was increased from 3.36 to 5.62, and the maximum lift coefficient for full flaps and idle power was increased from 2.23 to 4.40. The suction boundary-layer system required 5.4 hp for its operation.

V. Other Boundary-Layer Studies

As discussed earlier, Cornish had noted in flight tests of both the TG-3A glider [10] and the L-21 [27] the existence of a laminar separation bubble very near the leading edge of the wing. In the tests of the L-21, this bubble had led to leading-edge stall, limiting the maximum lift coefficient that could be obtained with the L-21, even with distributed suction boundary-layer control. Two different studies examined ways of overcoming the problem of the laminar separation bubble. A study by Gyorgyfalvy [30] investigated the effectiveness of drooping the leading edge of the wing on the L-21. This was the same aircraft used by Cornish in his study [27] and had suction boundary-layer control applied in the range $0.15 < x/c < 1$. Figure 35 (Fig. 1 in [31]) shows the original nose shape and the two droop geometries studied. In the first geometry (top drawing), the nose droop resulted in a decrease in the leading-edge radius from $r/c = 0.02$ to $r/c = 0.015$. In the second geometry (bottom drawing), the drooped nose had an increased nose radius ($r/c = 0.028$). Pressure and velocity profile measurements were made at semispan locations $2y/b = 0.32$ (ahead of the flap) and $2y/b = 0.85$ (ahead of the aileron), as were maps of the separation bubble using a Stanton tube.

The increment in maximum lift coefficient $\Delta C_{L\max}$ obtained over the baseline value of 2.46 for the undrooped wing was 0.48 for the first droop geometry and 0.32 for the second droop geometry. The upper- and lower-surface pressure distributions for the original nose shape with zero flap deflection are shown in Fig. 36 (Fig. 5a in [31]). The pressure distributions measured on the modified wings revealed that the drooped leading edge 1) caused the stagnation point to move forward, 2) caused the position of the suction peak to move forward, 3) caused the magnitude of the suction peak to decrease, and 4) caused a sharper pressure peak to form at lower speeds which decreased in sharpness more rapidly as the airplane speed increased,

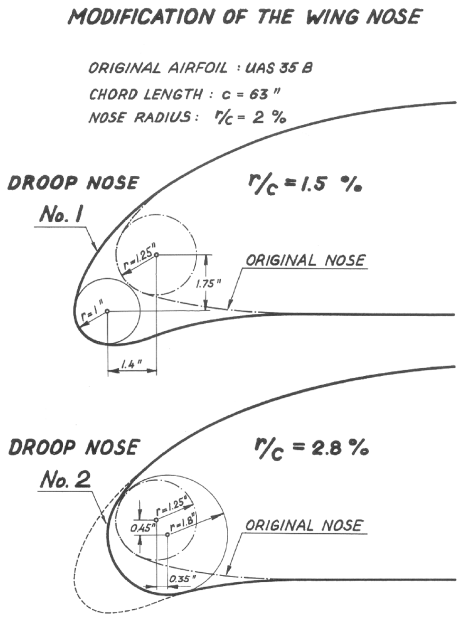

Fig. 35 Geometries of drooped leading edges on L-21 wing (Fig. 1 in [30]).

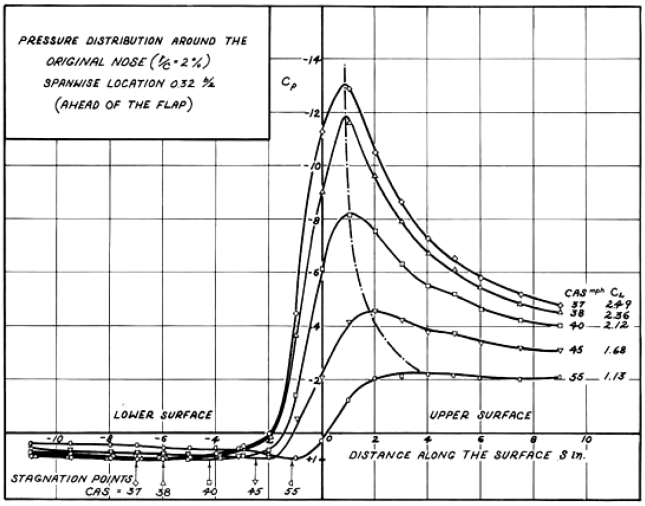

Fig. 36 Pressure distributions near leading edge of L-21 wing with no droop (Fig. 5a in [30]).

than for the undrooped leading edge. These behaviors can be understood fairly readily. At high lift coefficients and thus high angles of attack, the stagnation point is well back on the lower surface of the wing. The flow has to accelerate significantly in going around the leading edge of the wing to the upper surface. This means that the pressure drops dramatically, creating a large suction peak. The rise in pressure that has to follow the suction peak leads to the creation of the laminar separation bubble. By drooping the leading edge, the stagnation point is moved nearer to the leading edge, decreasing the amount of acceleration that occurs in the flow going over the upper surface.

Figure 37 (Fig. 15c in [31]) maps the locations of the stagnation points, the suction peaks, and the extent of the laminar separation bubble for the second drooped leading edge for zero flap deflection. Gyorgyfalvy [30] noted from these and other results that the drooped leading edge led to a shorter bubble which began forming at lower speeds, implying a larger maximum lift coefficient. When the flap was deflected, the separation and reattachment points both moved forward. For the undrooped leading edge, the separation and reattachment locations moved forward roughly the same amount, so the length of the bubble did not change. For the second leading-edge droop geometry, the separation point moved forward a small amount when the flaps were deflected, but the reattachment point moved forward a much greater distance, so that the bubble length was reduced by approximately two-thirds. The tests of the undrooped leading edge and the second droop geometry were conducted

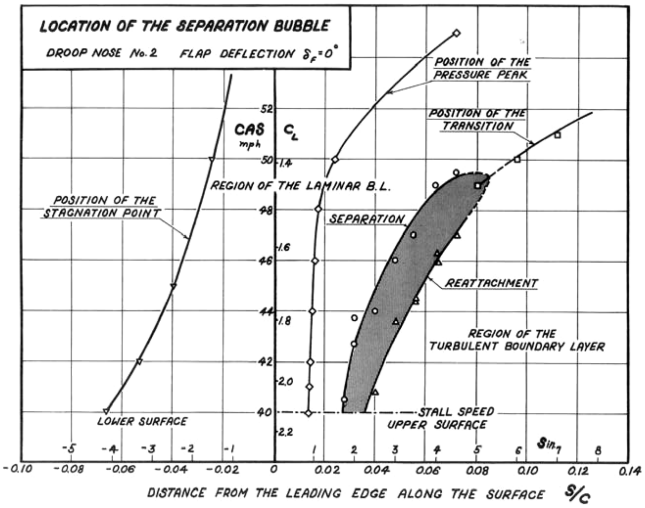

Fig. 37 Map of flow properties for second leading-edge droop geometry (Fig. 15c in [30]).

simultaneously. The left wing of the L-21 had the undrooped leading edge, and the right wing had the second droop geometry applied. For the case of no flaps, the right wing stalled first, whereas with full flap deflection, the left wing stalled first. In both cases, the separation location on the stalled wing was further forward and the separation bubble on the stalled wing was longer. Gyorgyfalvy concluded that the droop nose could be a useful device for delaying laminar separation and leading-edge stall, within limits.

A second study [31] also concerned itself with the behavior of the laminar separation bubble. A wind tunnel was constructed to create a nominally two-dimensional boundary layer. The boundary layer developed on a hinged wall of the wind tunnel downstream of the contraction. The wall was deflected outward to create an adverse pressure gradient. For a wall angle of 17.5 deg at a throat velocity of 75 ft/s, the boundary layer separated at the corner of the hinged wall and reattached as a turbulent boundary layer 0.8 in. downstream of the separation point. Measurements of the flow upstream of the separation verified that the boundary layer was laminar at separation. Suction was applied to the hinged wall through 0.018-in-diam holes drilled in a square pattern with a separation of 0.1 in. between the hole centers. The holes were connected to suction chambers beneath the walls. The distribution of applied suction was accomplished by uncovering rows of holes within the suction chambers. The pressure inside the suction chambers was constant, and because the pressure in the freestream varied because of the change of tunnel area, the local pressure difference between the suction chamber and the flow varied along the wall. This variation resulted in a variation in the suction velocity along the wall. The suction velocity at a given hole row was determined from the known pressure difference at that location and a calibration of the flow rate through a hole of the same diameter through the same material as a function of pressure difference. The farthest downstream from the corner that the boundary layer could be surveyed was 3.88 in. The boundary layer was surveyed at this location with no suction applied and was found to be turbulent with a thickness of 0.55 in. This location was taken as a datum and the effects of suction on the downstream development of the boundary layer were measured at this point.

Initially, suction was applied in a narrow region downstream of the reattachment location. As the suction was extended forward into the region of the bubble, the bubble pressure coefficient became more negative and the bubble length decreased (see Fig. 38, which is Fig. 19 in [31]; in this figure, suction is a positive quantity and blowing is negative). For the fixed conditions at separation, the application of suction in general caused a decrease in the bubble pressure and length and a decrease in displacement and momentum thicknesses at the downstream datum location. The boundary-layer properties at the downstream datum location were in fact functions only of the total flow rate removed from the flow by the suction. The shape factor H of the boundary layer at the datum location depended only upon the total suction rate Q, with the results for all five different suction distributions collapsing onto a single curve of H as a function of Q. Based on their studies, Burrows and Newman were able to offer a possible explanation for the results observed by Cornish. In their studies, the separation location was fixed at the wall corner. In a case where the separation location is not fixed, such as on an airfoil, Burrows and Newman speculated that the reduction of bubble pressure by suction could cause a slight forward motion of the separation bubble. This forward motion could in turn cause a reduction in the boundary-layer Reynolds number based on displacement thickness, and the bubble could switch from a "short" bubble to a "long" bubble, leading to leading-edge stall.

The goal of much of the boundary-layer research by Raspet and his coworkers had been the development of short takeoff and landing aircraft. The improvements to the takeoff performance of the L-21 with suction boundary-layer control have already been noted [27]. However, as was also noted in those studies, the climbout performance at the low takeoff speed was much less than the climbout performance at higher speeds, implying less improvement in overall takeoff distance than might otherwise have been expected. The issue was the poor propeller performance at the lower speeds, and according to a survey paper [32] presented by Raspet, the answer was a ducted propeller. Raspet argued that the higher thrust available from a ducted propeller would help in overcoming the high induced drag experienced by STOL aircraft at low speeds where high lift is being generated. It was necessary for the ducted propeller to be placed on an aircraft in a pusher configuration, because a duct on a tractor configuration would be unstable aerodynamically in yaw. The design criteria for a ducted propeller were that the propeller would produce high thrust at low speeds and that the duct would not have high drag in cruising flight, implying that the thickness of the duct cross section must be kept small.

One of the key issues in duct design was the separation of the flow around the leading edge of the duct, due to what Raspet termed the centrifugal forces arising from the high curvature of the wall. The acceleration in the direction normal to the wall was approximated with the expression

$$\frac{a_y}{g} = \frac{1}{g}\left(\frac{U^2}{R} - \frac{1}{\rho}\frac{dp}{dy}\right) \tag{12}$$

It was noted that separation occurred at precisely the location where the normal acceleration changed signs, indicating that the separation was due to the lack of required centripetal acceleration toward the wall. The separation on a propeller duct inlet was observed with flow visualization in Fig. 39 (Fig. 4 in [32]), which was obtained by mounting a plate on the leading edge of the duct, perpendicular to the cross section of the duct, and injecting dye on the surface of the plate [33]. The movement of dye away from the duct surface illustrates the separation near the duct leading edge. This

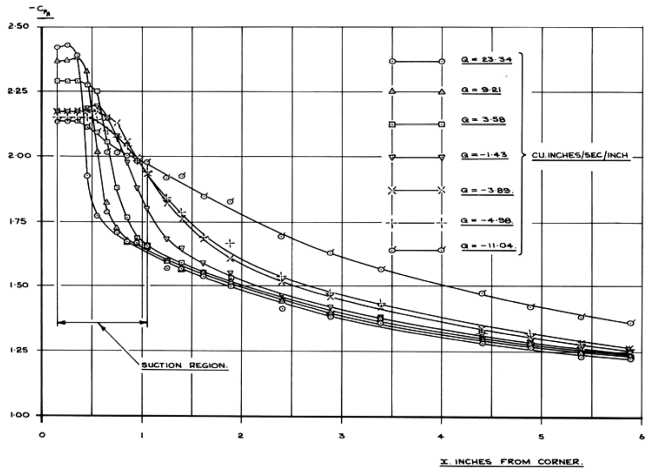

Fig. 38 Effects of suction on laminar separation bubble, long suction length (Fig. 19 in [31]; reattachment length was 0.8 in. for no suction).

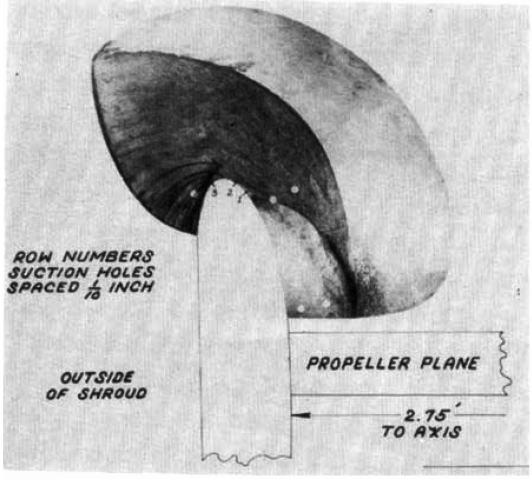

Fig. 39 Flow visualization of separation on propeller duct inlet; flow direction is from top to bottom in figure (Fig. 4 in [32]).

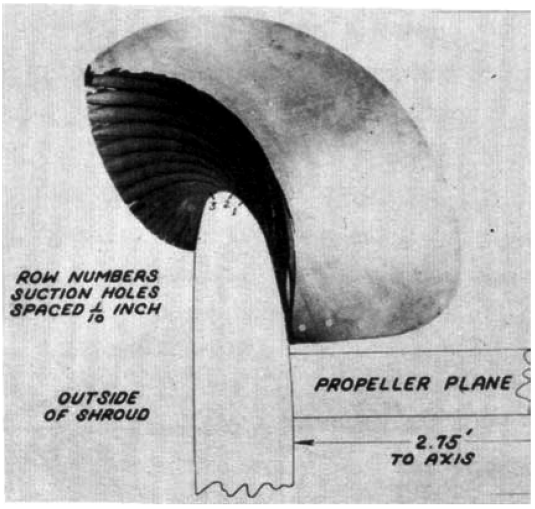

Fig. 40 Flow visualization of attached flow on propeller duct inlet with suction boundary-layer control; flow direction is from top to bottom in figure (Fig. 8 in [32])

Fig. 41 Anderson–Greenwood AG-14 with shrouded propeller (Fig. 13 in [33]).

separation was detrimental to the propeller performance because it meant that the propeller tip was stalled, creating a tip vortex that caused a large induced drag on the propeller blade which in turn resulted in poor propeller efficiency at low speeds. The issue of separation on the duct was addressed in two ways. The first was through a redesign of the duct cross-sectional profile. Profiles with cambered elliptic cross sections and with an axisymmetric Borda mouthpiece cross section were designed and tested, yielding higher values of the centripetal acceleration toward the wall. Suction was also applied to the leading edge of the original duct cross section, and the resulting attached flow is shown in Fig. 40, indicating the effectiveness of the suction boundary-layer control.

The establishment of attached flow on the duct surface led to a different problem with the propeller. The flow at the propeller tip was now a high-velocity flow, and for the propeller with a conventional twist distribution, the high velocity at the tip meant a low angle of attack, with the result that the end of the propeller was essentially windmilling and producing little thrust. A study of twist distributions of the propeller mounted on an AG-14 research aircraft with a shroud was conducted [34]. The airplane is shown in Fig. 41. The original

Fig. 43 XAZ-1 Marvellette.

twist distribution was such that at the 0.66 radius point, the twist was 4.2 deg and had a smaller value at the tip. The modified propeller had a constant chord and constant twist angle to the 0.9 radius point, where the twist was gradually increased to 7 deg at the tip. The results of the flight tests are shown in Fig. 42. The increase in velocity around the leading edge of the duct, in particular at the static thrust conditions, is significant, because it implies a lower pressure on the forward-facing areas of the duct, which contribute significantly to the thrust production of a ducted propeller. The modified twist distribution resulted in increases of 25% in both the propulsive efficiency and the thrust coefficient. Without the duct, the 90 hp engine and original propeller had produced a static thrust of 265 lb. With the duct and the modified propeller, the same engine produced 560 lb of static thrust. One drawback of adding the duct was that, at cruise conditions, the performance was not improved significantly, due to the drag of the duct and the conventional tail surface configuration. A suggested remedy was eliminating the separate tail surfaces by applying the tail control surfaces to the duct.

VI. Conclusions

In his boundary-layer research and in that of the engineers and students working under him, Raspet had methodically worked toward the development of STOL aircraft technology. The concept of distributed suction boundary-layer control for the prevention of separation had been developed and used to increase the maximum lift coefficients of gliders and powered aircraft. The use of a ducted propeller to increase thrust at low speeds had been demonstrated, and its performance improved by the application of suction boundary-layer control to the duct and by adjusting the propeller twist distribution. The sealed flap which effectively varied the camber of the wing had been developed. In 1958, Raspet and his team received a contract from the U. S. Army to develop a STOL aircraft [35]. A technology demonstrator, the XAZ-1 "Marvellette" (Fig. 43) first flew in 1962 [35]. It was followed by the XV-11A MARVEL (for Mississippi aerophysics research vehicle with extended latitude, shown in Fig. 44), which first flew in December of 1965 and had the distinction of being the world's first all-composite aircraft [35]. Unfortunately, August Raspet did not live to see these fruits of his labors. He was at the controls in April of 1960 when a Piper Super Cub with boundary-layer control crashed while he was demonstrating it for Lowell L. Meyer, a representative of the Chance–Vought Aircraft Corporation [36]. Both Raspet and Myer were killed in the crash.

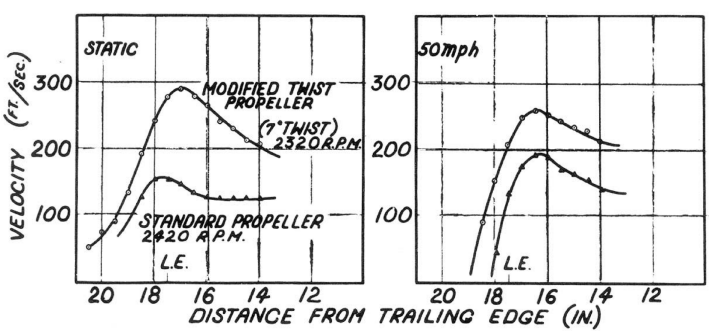

Fig. 42 Effects of propeller twist on surface velocity distribution on leading edge of duct (Fig. 10 in [32]).

Fig. 44 XV-11A MARVEL.

Some of the issues addressed by Raspet and his coworkers are still subjects of study. Premature transition caused by a laminar separation bubble is still a factor in applications ranging from laminar flow control airfoils [37] to the design of an inlet for a quiet Mach 6 Ludwieg tube [38]. The instability of the laminar boundary layer resulting from the application of too much suction (or "oversuction") was explained by Goldsmith [39] in 1957 as the result of secondary flows induced by the suction, as had been conjectured by Carmichael [6]. Experiments conducted by Anselmet et al. [40] further confirmed the fact that oversuction could trigger transition, although the specific mechanisms leading to transition were still being examined as late as 2003 [41]. Today, in research that makes a striking parallel to Raspet's work, low-speed flight tests are being conducted by Saric [42] in pursuit of the goal of laminar flow control on swept wings.

References

[1] Haug, C. J., *Mechanical Feature: 100 Years of Engineering at Mississippi State University*, Univ. Press of Mississippi, Jackson, MS, 1992, Chap. 5.

[2] Barnett, J. C., "Building Rockets on the Moon: A History of the Department of Aerospace Engineering at Mississippi State University, 1933–1960," M.A. Thesis, Dept. of History, Mississippi State Univ., Dec. 2001.

[3] Raspet, A., "Flight Measurements of Automatic Trailing Edge Suction on a Sailplane," Mississippi State College, Research Rept. 3, Engineering Research Station, 30 Sept. 1952.

[4] Cornish, J. J., III, "Some Aerodynamic and Operational Problems of STOL Aircraft with Boundary-Layer Control," *Journal of Aircraft*, Vol. 2, No. 2, 1965, pp. 77–86.

[5] Cornish, J. J., III, "Experimental Techniques for Analyzing the Turbulent Boundary Layer," Mississippi State College, Research Rept. 8, Aerophysics Dept., 7 Oct. 1954.

[6] Raspet, A., "Mechanism of Automatic Trailing Edge Suction," Mississippi State College, Research Rept. 1, Engineering Research Station, 31 Dec. 1951.

[7] Raspet, A., "Sailplane as a tool for Boundary Layer Research," *50 Jahre Grenzschichtforschung*, edited by Goertler, H., and Tollmien, W., Viewig, Brunswick, Germany, 1955, pp. 487–499.

[8] Carmichael, B. H., "Summary of Flight Research on Nineteen Porosity Distributions Designed to Maintain Laminar Boundary Layers on a NACA Airfoil with a Single Internal Chamber," Mississippi State College, Research Rept. 6, Aerophysics Dept., 13 Oct. 1953 (revised 1 May 1954).

[9] Carmichael, B. H., "Flight Observations of Suction Stabilized Boundary Layers," Mississippi State College, Research Rept. 4, Engineering Research Station, 20 Jan. 1953.

[10] Cornish, J. J., III, "Prevention of Turbulent Separation by Suction Through a Perforated Surface," Mississippi State College, Research Rept. 7, Engineering Research Station, 13 Oct. 1953.

[11] Raspet, A., "Boundary Layer Studies on a Sailplane," *Aeronautical Engineering Review*, Vol. 11, No. 6, 1952, pp. 52–60.

[12] Betz, A., "Generalization of the Joukowsky Conformal Transformation," *Zeitschrift fur Flugtechnik und Motorluftshiffahrt*, Vol. 15, No. 10, 1924, pp. 100–104.

[13] Regenscheit, B., "Automatic Suction," *Thermik*, Vol. 3, No. 11, 1950, pp. 175–179.

[14] Smith, C. B., "Solution for the Lift and Drag of Airfoils with Air Inlets and Suction Slots," *Journal of the Aeronautical Sciences*, Vol. 16, No. 10, 1949, pp. 581–589.

[15] Ulrich, A., "Theoretical Investigation of Drag Reduction in Maintaining the Laminar Boundary Layer by Suction," NACA TM 1121, June 1947.

[16] Schlichting, H., "Approximate Method for Calculation of the Laminar Boundary Layer with Suction for Bodies of Arbitrary Shape," NASA TM 1216, March 1949.

[17] Iglisch, R., "Exact Calculation of Laminar Boundary Layer in Longitudinal Flow over a Flat Plate with Homogeneous Suction," NASA TM 1205, April 1949.

[18] Pfenninger, W., "Investigations on Reductions of Friction on Wings, in Particular by Means of Boundary Layer Suction," NACA TM 1181, Aug. 1947.

[19] Pfenninger, W., "Experiments on a Laminar Suction Airfoil of 17 Percent Thickness," *Journal of the Aeronautical Sciences*, Vol. 16, No. 4, 1949, pp. 227–236.

[20] Burrows, D. L., Braslow, A. L., and Tetervin, N., "Experimental and Theoretical Studies of Area Suction for the Control of the Laminar Boundary Layer on a Porous Bronze NACA 64A010 Airfoil," NACA TN 1905, 1949.

[21] Braslow, A. L., Burrows, D. L., Tetervin, N., and Visconti, F., "Experimental and Theoretical Studies of Area Suction for the Control of the Laminar Boundary Layer on a Porous Bronze NACA 64A010 Airfoil," NACA Report 1025, March 1951.

[22] Carmichael, B. H., "Flight Observations of Suction Stabilized Boundary Layers," *Aeronautical Engineering Review*, Vol. 13, No. 2, 1954, pp. 36–41.

[23] Squire, H. B., and Young, A. D., "Calculation of the Profile Drag of Aerofoils," Aeronautical Research Council Repts. and Memoranda No. 1838, 1938.

[24] Thwaites, B. (ed.), *Incompressible Aerodynamics*, Dover, New York, 1987; reprint, Oxford Univ. Press, Oxford, England, U.K., 1960, pp. 180–181.

[25] Raspet, A., "Momentum Conservation in Boundary Layer Control," presented at *Boundary Layer Control Symposium*, Naval Ordnance Lab., White Oaks, MD, 24 June 1953.

[26] McCullogh, G. B., and Gault, D. E., "Experimental Investigation of the NACA 631-012 Airfoil Section with Leading Edge Suction Slots," NACA TN 1683, Aug. 1948.

[27] Raspet, A., Cornish, J. J., III, and Bryant, G. D., "Delay of the Stall by Suction Through Distributed Perforations," Dept. of Aerophysics, Mississippi State College; reprint of paper presented at *24th Annual Meeting of the Institute for Aeronautical Sciences*, 23–26 Jan. 1956.

[28] Raspet, A., Cornish, J. J., III, and Bryant, G. D., "Delay of the Stall by Suction Through Distributed Perforations," *Aeronautical Engineering Review*, Vol. 15, No. 8, 1956, pp. 32–39.

[29] Cornish, J. J., III, "Practical High Lift Systems Using Distributed Boundary Layer Control," Aerophysics Dept., Mississippi State Univ., Research Rept. No. 19, 10 Dec. 1958.

[30] Gyorgyfalvy, D., "Flight Research Investigation of Laminar Separation of a High Lift Boundary Layer Control Airplane," Aerophysics Dept., Mississippi State Univ., Research Rept. No. 25, 26 June 1959.

[31] Burrows, F. M., and Newman, B. G., "Application of Suction to a Two-Dimensional Laminar Separation Bubble," Aerophysics Dept., Mississippi State Univ., Research Rept. No. 27, 1 Oct. 1959.

[32] Raspet, A., "Ducted Propeller for STOL Airplanes," American Society of Mechanical Engineers, Paper 60-AV-11, June 1960.

[33] Claybourne, M. M., "Study of a Shrouded Propeller with Distributed Suction on the Inlet Profile," Aerophysics Dept., Mississippi State Univ., Research Rept. No. 24, 10 Dec. 1958.

[34] McNay, D. E., "Study of the Effects of Various Propeller Configurations about a Shroud," Aerophysics Dept., Mississippi State Univ., Research Rept. No. 14, Feb. 1958.

[35] Roberts, S. C., Stewart, D., Mertaugh, L., Boaz, V., Wells, G., Bryant, G., and Gaddis, M., "XV-11A Description and Preliminary Flight Test," Aerophysics Dept., Mississippi State Univ., Research Rept. No. 75, April 1967.

[36] Bridges, D. H., "Aeronautics, Aerophysics, and Aerospace: A History of Aerospace Engineering at Mississippi State University," *Aerospace Engineering Education During the First Century of Flight*, edited by McCormick, B., Newberry, C., and Jumper, J., AIAA, Reston, VA, 2004, pp. 328–350.

[37] Saric, W. S., and Reed, H. L., "Toward Practical Laminar Flow Control: Remaining Challenges," AIAA Paper 2004-2311, June 2004.

[38] Taskinoglu, E. S., Knight, D. D., and Schneider, S. P., "Computational Fluid Dynamics Evaluation of Bleed Slot of Purdue Mach 6 Quiet Tunnel," *Journal of Spacecraft and Rockets*, Vol. 44, No. 6, June 2006, pp. 1360–1362.

[39] Goldsmith, J., "Critical Laminar Suction Parameters for Suction into an Isolated Hole or a Single Row of Holes," Northrop Aircraft, Rept. No. NAI-57-529 (BLC-95), 1957.

[40] Anselmet, F., Merigaud, E., and Fulachier, L., "Effect of Hole Suction

on Boundary Layer Transition," *Proceedings of the First European Forum on Laminar Flow Technology, Hamburg, March 16–18, 1992*, German Society for Aeronautics and Astronautics Rept. 92-06, 1992, pp. 67–72.

[41] Messing, R., and Kloker, M., "DNS Study of Discrete Suction in a 3-D Boundary Layer," *Recent Results in Laminar-Turbulent Transition (Notes on Numerical Fluid Mechanics and Multidisciplinary Optimization)*, edited by S. Wagner, M. Kloker, and U. Rist, Vol. 86, Springer, New York, 2003, pp. 177–188.

[42] Saric, W. S., "Final Report: Swept Wing In-Flight Testing (SWIFT)," Texas A&M Univ., TAMUS-AE-TR-06-004, College Station, TX, 12 June 2006.